Drug Delivery and Translational Research (2023) 13:3094–3131
https://doi.org/10.1007/s13346-023-01375-y

ORIGINAL ARTICLE

Quality by design–based development and optimization of fourth-generation ternary solid dispersion of standardized *Piper longum* extract for melanoma therapy

Debadatta Mohapatra[1] · Dulla Naveen Kumar[2] · Singh Shreya[1] · Vivek Pandey[3] · Pawan K. Dubey[3] · Ashish Kumar Agrawal[2] · Alakh N Sahu[1]

Accepted: 25 May 2023 / Published online: 9 June 2023

Abstract

The study aimed to enhance the solubility, dissolution, and oral bioavailability of standardized *Piper longum* fruits ethanolic extract (PLFEE) via fourth-generation ternary solid dispersion (SD) for melanoma therapy. With the use of solvent evaporation method, the standardized PLFEE was formulated into SD, optimized using Box-Wilson's central composite design (CCD), and evaluated for pharmaceutical performance and in vivo anticancer activity against melanoma (B16F10)–bearing C57BL/6 mice. The optimized SD showed good accelerated stability, high yield, drug content, and content uniformity for bioactive marker piperine (PIP). The X-ray diffraction (XRD), differential scanning calorimetry (DSC), polarized light microscopy (PLM), and selected area electron diffraction (SAED) analysis revealed its amorphous nature. The attenuated total reflectance-Fourier transform infrared spectroscopy (ATR-FTIR) and high-performance thin layer chromatography (HPTLC) revealed the compatibility of excipients with the PLFEE. The contact angle measurement and in vitro dissolution study revealed excellent wetting of SD and improved dissolution profile as compared to the plain PLFEE. The in vivo oral bioavailability of SD reflected a significant ($p < 0.05$) improvement in bioavailability ($F_{rel} = 188.765\%$) as compared to plain extract. The in vivo tumor regression study revealed the improved therapeutic activity of SD as compared to plain PLFEE. Further, the SD also improved the anticancer activity of dacarbazine (DTIC) as an adjuvant therapy. The overall result revealed the potential of developed SD for melanoma therapy either alone or as an adjuvant therapy with DTIC.

Keywords Solid dispersion · Optimization · *Piper longum* · Dissolution · Bioavailability · Melanoma

Introduction

Melanoma, a most aggressive and deadly form of skin cancer, arises from the malignant transformation of melanocytes. As per National Cancer Institute (NCI) epidemiology survey, melanoma is the 5th most common cancer in USA with an estimated 97,610 new cases and 7,990 deaths in 2023 [1]. Data from the Global Cancer Observatory (GCO) shows that the annual incidence of melanoma cancer in both sexes in 2020 was 3,24,635 cases worldwide, with the highest number recorded in Europe (150,627), followed by Northern America (105,172), Asia (23,753), Oceania (19,239), Latin America and the Caribbean (18,881), and Africa (6963) [2]. Fair-skinned Caucasian populations are more prone to melanoma; however, its occurrence in pigmented populations in Asia and Africa has also been noticed on the nail beds, mucous membranes, and soles of the feet at a low incidence rate [3, 4]. The most prevalent type of melanoma is cutaneous melanoma which appears on the cutaneous surface [5, 6]. Although melanoma is regarded as multifactorial, the major risk factor is excessive exposure to ultraviolet (UV) radiation, which causes genetic mutations, and DNA damage, and mediates inflammatory responses [3, 4, 6]. In

✉ Alakh N Sahu
ansahu.phe@iitbhu.ac.in

1 Phytomedicine Research Laboratory, Department of Pharmaceutical Engineering & Technology, IIT (BHU), Uttar Pradesh, Varanasi 221005, India

2 Nanomedicine Research Laboratory, Department of Pharmaceutical Engineering & Technology, IIT (BHU), Uttar Pradesh, Varanasi 221005, India

3 Centre for Genetics Disorders, Institute of Science (BHU), Uttar Pradesh, Varanasi 221005, India

addition, other factors like numerous freckles, increased number or size of melanocytic nevi, pre-existing dysplastic nevus, decreased DNA repairability, tanning inability, suppressed immune system, mutations in cyclin-dependent kinase 4 (CDK4), and cyclin-dependent kinase inhibitor 2A (CDKN2A or p16) participate in development and progression of melanoma [4, 6]. The hyperactivation of mitogen-activated protein kinase (MAPK) due to mutation in BRAF and NRAS genes and phosphatidylinositol-3-kinase (PI3K) by multiple factors leads to the development of melanoma [3, 7, 8]. The majorities of currently used chemotherapeutics possess narrow therapeutic window, induces toxicities, unwanted adverse events, suppression of the immune system, tissue damage (extravasation), and induces resistance [7, 9, 10]. High cost is another problem which restricts their widespread use.

Most of the chemotherapeutic agents (90%) are administered in the palliative setting to stabilize the disease or to improve the quality of life. About 60 to 70% of anticancer chemotherapeutic agents are derived from natural origin, reflecting the potential of natural products in cancer therapy [10]. Many plant-derived drugs such as paclitaxel, taxol, camptothecin, irinotecan, vinblastine, and vincristine have been approved by FDA for the treatment of various cancer [11–13]. Plant-based substances have a wide range of structural and biological activities, as well as low toxicity, making them crucial for pharmaceutical research [14]. The plant-derived medicaments can be used as an alternative and supportive therapy to the current chemotherapeutics for melanoma. Numerous plant extracts and phytoconstituents have been well exploited for melanoma therapy for their ability to suppress melanoma through the regulation of oxidative status, modulation of immunity, correction of disordered replication and induction of apoptosis, prevention of invasion, angiogenesis, and metastasis [3, 15]. Multiple mechanisms are involved in the development, progression, invasion, angiogenesis, and metastasis of melanoma. Hence, it is rational to use plant extract or fraction (comprising numerous phytoconstituents) that may act synergistically in a multi-targeting manner rather than a single constituent or drug molecule.

The fruits of *Piper longum* (Long pepper, Family: Piperaceae) have several medicinal properties, including anticancer, immunomodulatory, antiinflammatory, hepatoprotective, and melanin-inhibiting activity [16]. Major constituents of fruit include alkaloids (e.g., piperine (PIP), piperlonguminine (PLGN), piperlongumine, pellitorine), lignans, esters, volatile oils, and organic acids [16].

The major active component of *P. longum*, the PIP has been reported for its anticancer activity against melanoma, cervical carcinoma, adenocarcinoma, breast cancer, oral squamous cell carcinoma, prostate cancer, and hepatocellular carcinoma through various in vitro and in vivo tumor models [17]. In a recent ongoing clinical trial (Phase I), a combination of curcumin and PIP (standardized extract) is used to reduce inflammation for ureteral stent–induced symptoms in patients with cancer [18]. In another ongoing clinical trial (Phase II), a combination of curcumin and PIP is being studied in patients to determine whether the combination of supplements can prevent or delay the progression of prostate cancer, monoclonal gammopathy of unknown significant, or low-risk smoldering myeloma into a more aggressive cancer [18]. The extract of fruit as well as its constituents has shown their anticancer activity against melanoma. PIP inhibits transcription factors, such as cyclic AMP response element-binding protein (CREB), activated protein-1 (AP-1), nuclear factor-kβ (NF-kβ), and proinflammatory cytokine gene expression (IL-6, IL-1β, GM-CSF, and TNF-α) in B16F10 (melanoma) cells [19]. It also causes G1 phase arrest and apoptosis induction in B16F0 and SK MEL 28 melanoma cells through activation of checkpoint kinase-1 [20]. The PIP was also studied for inhibition of lung metastasis in the B16F10 cell–induced tumor model in C57BL/6 mice [21]. Piperlongumine was reported to produce cytotoxicity against human melanoma (A375, A875) and murine melanoma (B16F10) and induce apoptosis via reactive oxygen species–mediated disruption of mitochondria [22]. The PLGN was also reported to suppress melanogenesis via the downregulation of tyrosinase expression in the melanin synthesis pathway [23], and inhibition of melanogenesis seems a rational adjuvant approach for the treatment of metastatic melanoma [24]. The ethanolic extract of fruit was also examined both in vitro and in vivo for antiangiogenic properties via inhibition of vascular endothelial growth factor (VEGF), tumor-directed capillary formation, and inhibition of proinflammatory cytokines [25]. Irrespective of wide significance, its therapeutic utility is restricted due to the low water solubility, limited dissolution, and in vivo oral bioavailability of the majority of active constituents [26–28]. Thus, the use of appropriate techniques to evade the solubility, dissolution, and bioavailability issues is extremely crucial to realize the actual therapeutic effectiveness.

Multiple formulation strategies, such as micronization, salt formation, solid dispersion, nanocrystalization, micro/nanoemulsion, pH modification, use of cosolvent, surfactant, micellar solubilization, lipid-based formulation, cyclodextrin complexation, cocrystallization, liquisolid technique, and nanoparticles encapsulation have been well exploited to avoid solubility issues [29–31]. Solid dispersion (SD) is one of the solid units of oral dosage form that possess the ability to overcome the solubility and bioavailability-related issues of poorly water-soluble drug candidates [32]. Due to the diversity of formulation methodology and a wide variety of excipient options, it has been realized as one of the most successful formulation

strategies. Oral administration of anticancer medications is most frequently used due to better patient compliance (easier administration, feasibility for repeated drug administration, independence, pain-free administration), home-based therapy, decreased risk of infections, better tolerability, limited severity of toxicity, and lower cost of therapy [33]. The SD allows homogeneous dispersion of drug candidate in the carrier matrix (CM) in a molecular, amorphous, microcrystalline, or colloidal state, which leads to the increased effective surface area, dispersibility, wetting ability, porosity, maintenance of supersaturation, dissolution, and improved oral bioavailability [31, 33–36].

Formulation methods, such as fusion or melting, solvent methods (e.g., freeze drying, spray drying, and rotatory evaporation), and melting-solvent methods are widely used for SD preparation; however, other advanced techniques like KinetiSol® dispersing (KSD), hot-melt extraction (HME), supercritical fluid (SCF) method, electrospinning spinning, co-precipitation technique, and microwave irradiation also used nowadays in industrial scale [31, 34, 36, 37]. The process of formulation should be affordable, safe, and rid of the usage of expensive machinery. Considering these factors, the solvent method via rotary evaporation is more beneficial for the lab-scale formulation of SDs. The use of a non-toxic solvent (Class III and Class IV) is essential for avoiding solvent-related toxicities during the use of the solvent evaporation method [32].

The current study aims to prepare ternary SD of standardized *Piper longum* extract via solvent-based rotary evaporation technique and characterize its pharmaceutical properties and evaluate its anticancer activity against melanoma. High-performance liquid chromatography (HPLC) was used to achieve the marker-based standardization of the PLFEE concerning PIP and PLGN to maintain batch-to-batch consistency and provide dose uniformity. The response surface methodology (RSM) and optimization were implemented to achieve highly efficient formulation with high saturation solubility. The proposed formula was formulated, and the outcome was verified to validate the software's optimized formula. The optimized *Piper longum* fruits ethanolic extract solid dispersion was characterized for percentage yield, drug content, content uniformity, moisture content, micromeritics properties (density, flow property), surface morphology (high-resolution scanning electron microscopy (HRSEM)), crystallinity (X-ray diffraction (XRD) and polarized light microscopy (PLM)), thermal behavior (differential scanning calorimetry (DSC) and thermogravimetric analysis (TGA)), drug-excipient compatibility (attenuated total reflectance-Fourier transform infrared spectroscopy (ATR-FTIR) and high-performance thin layer chromatography (HPTLC)), in vitro dissolution, stability (long term and accelerated), in vivo oral bioavailability, and for anticancer activity against melanoma (B16F10)–bearing C57BL/6 mice.

Materials and methods

Materials

Fruits of *Piper longum* (*P. longum*) were collected from a local herbal market (Varanasi, Uttar Pradesh, India). PIP (MW: 285.34 g/mol, ≥ 97% purity), hydroxypropyl cellulose (HPC, Avg MW: 80,000), Poloxamer 407, Dulbecco's Modified Eagle's Medium (DMEM/F-12), and fetal bovine serum (FBS) were purchased from Sigma-Aldrich (St. Louis, MO, USA). PLGN (MW: 273.3 g/mol, ≥ 98% purity) was procured from Cayman Chemical Company (Michigan, USA). The p-dimethylaminobenzaldehyde (p-DMAB) was obtained from Spectrochem Private Limited (Mumbai, India). Tween® 20 (MW:522.7 g/mol, HLB value: 16.7), polyethylene glycol 4000 (PEG-4000), and polyethylene glycol 9000 (PEG-9000) were purchased from Sisco Research Laboratory (Mumbai, India). Kolliphor® P 188 (Avg MW: 7680 to 9510 g/mol, HLB value: ~ 29.0), Soluplus® (Avg MW: 90,000 to 140,000 g/mol, HLB value: ~ 14.0), and Kolliphor® RH 40 (HLB value: 14–16) were gifted by BASF Corporation (Ludwigshafen, Germany). Gelucire® 44/14 (HLB value: 11–14) was provided as gift samples by Gattefosse (Saint-Priest, Cedex, France). Tween® 80 (MW: 1310 g/mol, HLB value: 15.0) was obtained from SD Fine-Chem Limited (Mumbai, India). Empty gelatin capsules (size 00) were obtained from Pacto Pharmaceuticals Ltd. Ethanol was purchased from Merck Chemicals (Darmstadt, Germany). Dacarbazine or dimethyl-triazeno-imidazole carboxamide (DTIC, IP, 99.54% purity) was kindly provided by Neon Laboratories Ltd., Mumbai, India, as a gift sample. HPLC grade methanol (Finar Limited, Ahmedabad, India) and water (Type-I HPLC grade water, obtained from Laboratory-grade Water Purification Systems, arium® mini, Sartorious, Sartorius Lab Instruments, Germany) were used as mobile phase for HPLC analysis. Dulbecco's Modified Eagle's Medium (DMEM/F-12), fetal bovine serum (FBS), MTT reagent (3-(4, 5-dimethylthiazol- 2-yl)-2, 5-diphenyltetrazolium bromide), and dimethyl sulfoxide (DMSO) were obtained from Sigma-Aldrich, St. Louis, MO, USA. All other analytical-grade chemicals were purchased from a standard supplier and used in the experiment without additional processing or purification. Double-distilled and type-I ultra-pure water was used throughout the studies as per the necessities. Membrane filters (0.45 µm cellulose nitrate) and syringe filters (polyvinylidene fluoride or PVDF, 0.2 µm) were obtained from AXIVA Sichem Pvt. Ltd., New Delhi, India. Kit for biochemical analysis was purchased from ARKRAY Healthcare Pvt. Ltd. (Mumbai, India).

Authentication of fruits, extraction, and residual solvent content of the extract

The collected fruits of *P. longum* were authenticated by Prof. N.K Dubey, Department of Botany, Institute of Science, Banaras Hindu University, and the voucher specimen (Pipera.2021/6) was deposited in the Departmental Herbarium. Further, the authenticity of the fruit was verified by DNA-based molecular characterization. The online Basic Local Alignment Search Tool (BLAST) study (NIH, National Library of Medicine, USA) was executed for the investigation of nucleotides sequence homology with authenticated sequences of ribulose-bisphosphate carboxylase gene (rbcL). The detailed experimental procedure has been provided in a supplementary file (Section 1.1). The collected fruits of *P. longum* were dried at room temperature. The dried fruits were coarsely powdered using a mixture grinder (HL7756/00, Phillips, India) and extracted via microwave-assisted exposure of crude powdered drugs at 450 W for 5 min (MC35J8085PT/TL, domestic microwave oven, HOTBLAST™, Samsung, South Korea) followed by triple maceration by soaking the partially grounded *P. longum* with absolute ethanol at a proportion of powder to solvent 1:4 w/v. Briefly, 1.2 kg of microwave-exposed dried powder of *P. longum* was soaked with 4.8 L of absolute ethanol and macerated for 72 h. The extraction was facilitated by placing the crude drug–solvent dispersion on an orbital shaker (REMI, RS 12 plus). Then, it was filtered through a vacuum membrane filter (pore size: 0.45 µM, diameter: 47 mm), and the filtrate (4.7 L) was collected and stored. The mark of the 1st extraction was further macerated twice (each of 72 h) with 1:4 w/v of absolute ethanol and filtered to yield the filtrate (9.4 L). The filtrates of all maceration events were mixed thoroughly to produce a total volume of 14.1 L. Batch wise, 500 mL of the final filtrate was concentrated in a rotary vacuum evaporator (IKA®, RV 10 digital, vacuum pump: IKA® MVP 10 basic, water bath: IKA® HB10 digital, and chiller system: IKA® RC 2 Basic) at 40 °C with 60 rpm and the concentrated extract was kept in a separate container. The obtained concentrated extract of each batch was added to the previously collected extract in a single container. After completion of all batches, the product was mixed thoroughly by glass rod to maintain the drug content uniformity and again subjected to a rotary vacuum evaporator for 15 min at 40 °C with 60 rpm. After the complete removal of solvent, the extract was collected and stored in a refrigerator until used. The extraction yield of PLFEE was calculated by Eq. (1).

$$\%\ Extraction\ yield = \frac{Weight\ of\ extract\ obtained}{Weight\ of\ powdered\ P.\ longum\ taken} \times 100 \quad (1)$$

The GC-HS analysis was performed for the analysis of residual ethanol in the PLFEE using a GC-HS instrument (7890, Agilent, USA) equipped with a headspace injector, CombiPAL automatic headspace sampler, capillary column (HP-5, 30 m length, 0.25 µm film thickness, and 0.28 mm id), temperature-controlled oven, capillary flow technology (CFT), and a flame ionization detector (FID). The details of the procedure were given in the supplementary file (Section 1.2).

High-performance liquid chromatography

The analysis was performed by an Agilent HPLC system (Agilent 1260 Infinity II, Agilent, USA) equipped with a quaternary pump (1260 Quat Pump VL), diode array detector (1260 DAD WR), autosampler (1260 Vial Sampler), column (Quasar™ C18 LC column, PerkinElmer, 250 × 4.6 mm with 5 µm particle size), a standard flow cell (13 µL, 10 mm, and 120 bar), and Open LAB CDS EZChrom Workstation VL software. The isocratic elution was executed at a flow rate of 1.00 mL/min using HPLC grade methanol and water (Finar Limited, India) as mobile phase at a ratio of 80:20 v/v with a run time of 10 min. Quantification of two markers, i.e., PIP and PLGN, was carried out by the developed HPLC method at their respective absorption maxima (λmax of PLGN: 340 nm and PIP: 342 nm). The HPLC method was validated for linearity range, accuracy (% recovery), precision (repeatability and intermediate precision: intra-day and inter-day), the limit of detection (LOD), the limit of quantification (LOQ), robustness, and system suitability test as per International Conference on Harmonization (ICH Topic Q 2 (R1)). The detailed HPLC methodology and its validation protocol are supplied in the supplementary file (Section 1.3).

Standardization of PLFEE

Marker-based standardization was performed to quantify the amount of PIP and PLGN in the PLFEE. Detailed methodology for marker-based standardization of PLFEE is provided in the supplementary file (Section 1.4).

Screening of carrier matrix by phase solubility experiment

To choose the most suitable CM for SD formulation, the phase solubility of standardized PLFEE (mainly the PIP) was checked in an aqueous solution of different carriers using the protocol described by Higuchi and Connors [38]. Polymers (Kolliphor P 188, hydroxypropyl cellulose, Poloxamer 407, Soluplus®, PEG-4000, PEG-9000, PVP k30) and surfactants (Gelucire® 44/14, Kolliphor® RH 40, Tween® 20, Tween® 80) were screened. An excess quantity of PLFEE (100 mg) was added to 1.5 mL of the aqueous solution of

CM at multiple concentrations (i.e., 2, 4, and 8% w/v) in micro-centrifuge tubes and vortexed for 5 min in a vertex mixture (SPINIX™ Vertex shaker, Tarsons Products Pvt. Ltd., Kolkata, India). All tubes were tightly closed, sealed to avoid solvent loss, and shaken for 48 h in a shaking water bath (Hindustan Apparatus Mfg., Mumbai, India) maintained at 37 ± 0.5 °C. Then, the samples were centrifuged (Remi CM 12 PLUS, Mumbai, India) at 10,000 rpm for 15 min. The supernatant was filtered through a 0.22-µm syringe filter and diluted suitably with HPLC grade methanol, and the concentrations of PIP were assayed by the validated HPLC method at 342 nm. All phase solubility tests were carried out in triplicate, and the data were presented as the average of three measurements. The Gibbs free energy equation (Eq. 2) was used to estimate the free energy transfer (ΔG_t°) of PIP from pure water to an aqueous polymeric or surfactant solution as follows [39–41]:

$$\Delta G_t^0 = -2.303RT\log\frac{S_c}{S_0} \tag{2}$$

where S_c/S_0 is the solubility ratio of PIP with aqueous polymeric or surfactant solution to that of neat water (without any polymer or surfactant). R is the universal gas constant, and T is the absolute temperature in Kelvin.

Formulation of SD incorporating PLFEE

Different SDs of standardized PLFEE were formulated by solvent evaporation method employing a rotary evaporator using Soluplus® and Tween® 80 as CMs. Briefly, a specified amount of PLFEE and CMs was solubilized in 2 mL ethanol and 10 mL of acetone, respectively. For complete solubilization, both solutions were sonicated in an ultrasonic bath (AN-SS-6L, GT SONIC®, at ultrasonic frequency: 40 kHz, and power: 150 W) for 10 min. Then, the solutions were mixed in a round bottom flask (100 mL) and sonicated at 25 ± 0.2 °C for definite periods (as per software-suggested formula) for the interaction of extract and CMs at a molecular level. Solvent evaporation was performed at 70 rpm using a rotary vacuum evaporator equipped with a vacuum pump and water bath at 50 °C . The film of SD was scrapped and dried in a vacuum desiccator for 24 h for the removal of residual solvent. The dried formulation was ground gently by a glass mortar and pestle and shifted through sieve # 60 to obtain uniform particle size. The obtained SD was kept in well-closed glass vials and stored in an anhydrous calcium chloride desiccator at room temperature. A physical mixture (PM) containing the composition of SD was prepared by simple intensive mixing of a definite quantity of PLFEE and CMs followed by gentle grinding with mortar and pestle until the formation of a homogenous product. Subsequently, the resultant mixture was sieved through mesh # 60 and kept in a well-closed glass container at room temperature for further characterization.

Quality by design (QbD) and optimization

Response surface methodology

In the present investigation, RSM was used to analyze the influence of critical material attributes (CMA), such as Soluplus® to PLFEE ratio (X_1, w:w) and Tween® 80 to PLFEE ratio (X_2, w:w), and critical process parameters (CPP), such as sonication time (X_3, min) on critical quality attributes (CQA), such as saturation solubility of PIP (Y_1) by applying a quality by design (QbD)–based approach using 3-factor, 5 levels rotatable (α value of 1.681) Box-Wilson central composite design (CCD) via a Trial version of Design-Expert® software (Version-12, Stat-Ease Inc., Minneapolis, MN, USA). A total of 20 runs (trial batches), including 6 replications of central points with 8 factorial points (cube points) and 6 axial points (star points), were produced by the software. The results of CQAs of 20 batches were fed into the software and analyzed by the inbuilt analysis of variance (ANOVA) tool to examine model adequacy and significance ($p < 0.005$) by comparing certain statistical constraints, such as correlation coefficient (R^2), model F-value, model p-value, lack of fit F-value, lack of fit p-value, the difference between predicted and adjusted R^2 value, and signal-to-noise ratio (adequate precision). To envisage the best SD, the statistical model was fitted to linear, two-factor (2F) interactions, quadratic, and cubic models. The software-generated mathematical polynomial equations were used to study multiple factors-response relationship. The interaction effect of the CMAs and CPP on the CQAs was also visualized using 3D response surface graphs and corresponding 2D contour plots.

The factor-responses relationship was estimated using a statistical polynomial Eq. (3) [42, 43].

$$Y = b_0 + b_1X_1 + b_2X_2 + b_3X_3 + b_{11}X_1^2 + b_{22}X_2^2 + b_{33}X_3^2 + b_{12}X_1X_2 + b_{23}X_2X_3 + b_{13}X_1X_3 \tag{3}$$

where Y is the response or dependent variable, X_1, X_2, and X_3 three different factors (independent variables), b_0 is Y intercept (a constant), and b_1, b_2, and b_3 are the linear or first-order coefficients for the factor X_1, X_2, and X_3 respectively. The terms b_{11}, b_{22}, and b_{33} are the quadratic or second-order coefficients of squared terms, such as ${X_1}^2$, ${X_2}^2$, and ${X_3}^2$. The interactive polynomial coefficients b_{12}, b_{23}, and b_{13} are associated with the interaction of multiple factors (X_1X_2, X_2X_3, and X_1X_3) during simultaneous analysis.

Optimization

Optimum CMAs and CPP required for the formulation of desired SD were acquired by numerical and graphical optimization techniques available in the software based on a set constrained condition of enhancing the saturation solubility of PIP (Y_1).

Check point analysis (validation of method)

The predictability/validity of the rotatable CCD model was verified by formulating a checkpoint batch ($n = 5$) of optimized formula under optimum circumstances as suggested by Design-Expert software and evaluating the corresponding CQAs (saturation solubility). Quantitative assessment between the software-based theoretical prediction and obtained experimental results was done by estimating the percentage prediction error (% Bias) by Eq. (4) [41, 43, 44].

$$\%\ prediction\ error = \frac{Experimental\ value - predicted\ value}{Predicted\ value} \times 100 \quad (4)$$

Characterizations of SD

Saturation solubility

The saturation solubility test was performed to evaluate the increase in the aqueous solubility of PIP in the formulated SD. Briefly, a surplus amount of standardized PLFEE (100 mg) and each SD (containing 100 mg standardized PLFEE) was mixed with 1.5 mL of water in a volumetric flask (10 mL). Samples were placed in triplicate on a thermostatically controlled oscillating water bath at 37 ± 0.5 °C for 48 h. Then, the samples were centrifuged at 10,000 rpm for 15 min, filtered through a 0.22-µm syringe filter, appropriately diluted with HPLC grade methanol, and investigated by the developed HPLC method at 342 nm. The results of saturation solubility were used for formulation optimization. Further, all the characterizations were done for optimized SD.

Drug content and content uniformity

The optimized SD equivalent to 100 mg of PLFEE was mixed with 10 mL of ethanol in a volumetric flask and sonicated for 10 min for complete solubilization. The solubilized sample was centrifuged (10,000 rpm for 15 min) and filtered (0.45 µm PVDF membrane filter). After suitable dilution, the drug content for PIP was estimated by HPLC. The % PIP content in the optimized SD was compared with that of an equivalent quantity of standardized PLFEE, considering its PIP content as 100%. The content uniformity was estimated by sampling from three different locations of optimized SD powder and estimating the variation in the PIP content. Each sample was analyzed in triplicate, and the average was reported.

Percentage yield

The yield of optimized SD was evaluated in triplicate to ascertain the efficiency of the solvent evaporation technique by comparing the mass of SD obtained to that of the initial weight of both standardized PLFEE and CMs using Eq. (5). The experiment was repeated in triplicate, and the average was reported.

$$\%\ Yield = \frac{Weight\ of\ prepared\ SD}{Weight\ of\ PLFEE + CM} * 100 \quad (5)$$

Micromeritics property

Micromeritic properties, like tapped density, bulk density, Carr's index, angle of repose, and Hausner's ratio, were investigated for prepared SD [45, 46]. Each of the experiments was carried out in triplicate, and the average was reported.

Angle of repose (Θ) A precisely weighed amount of SD was taken in a funnel and permitted to flow through it freely onto a flat surface to form a cone-shaped granular pile. The Θ was estimated using Eq. (6).

$$Angle\ of\ repose(\theta) = \tan^{-1}\frac{h}{r} \quad (6)$$

where h is the height of the cone and r is the radius of the cone base

Carr's compressibility index (CI) and Hausner's ratio (HR) A definite quantity of optimized SD was kept in a measuring cylinder of a digital tapped density apparatus (IKON Instruments, Delhi, India) to estimate tapped density. The cylinder was allowed to tap and the volume was noted at intervals of 10 taps. The tapped volume was considered when there was no alteration in volume after 3 consecutive readings. The bulk density was estimated by dividing the weight (g) by the bulk volume or volume without tapping (mL). The CI was calculated by using Eq. (7).

$$CI = \frac{Tapped\ Density - Bulk\ Density}{Tapped\ Density} \times 100 \quad (7)$$

The HR was calculated using Eq. (8)

$$Hausner\ ratio(HR) = \frac{Tapped\ Density}{Bulk\ Density} \quad (8)$$

X-ray diffraction

The crystallinity of PLFEE, CMs, PM, and SD was analyzed by a powder X-ray diffractometer (Rigaku Miniflex 600 Desktop System; Tokyo, Japan) using Ni-filtered Cu Kα radiation ($\lambda = 1.5406$ A°) at 40 kV voltage and 15 mA current. The diffraction pattern was recorded using MiniFlex Guidance software (Version 2.0.2.1) over a range of 2 Theta from 10 to 70° with a step size of 0.02°/step at a scan speed of 7°/min at 25 °C. Since Tween® 80 is viscus in nature, the drop cast technique was used to examine its XRD diffraction pattern by making a thin film on a glass plate via dropping and drying at 40 °C. Each of the experiments was carried out in triplicate to ascertain the consistency of the experimental outcome.

Differential scanning calorimetry

Thermal analysis ($n = 3$) of PLFEE, CMs, PM, and optimized SD was executed using DSC equipment (DSC 60 Plus, Shimadzu, Japan), furnished with TA-60WS Collection software (Version 2.21). Approximately 5 mg of each sample was kept in a pierced aluminum pan and placed in the thermal chamber. The study was performed from 20 to 300 °C at a linear heating rate of 10 °C/min in a nitrogen atmosphere at a flow rate of 100 mL/min. An empty pan was treated as the blank, and the instrument was calibrated with indium having a melting point of 156.6 °C.

Thermogravimetric analysis

TGA analysis ($n = 3$) of PLFEE, CMs, PM, and the SD was carried out using TGA apparatus (Shimadzu TGA-50 analyzer, Shimadzu, Japan) equipped with TA-60WS Collection software (Version 2.21). The analysis was conducted under a nitrogen atmosphere (flow rate of 100 mL/min) by linearly heating the samples (~ 7–10 mg) in a platinum pan from 10 to 800 °C at a heating rate of 10 °C/min.

Attenuated total reflectance-Fourier transform infrared spectroscopy

Infrared analysis ($n = 3$) of PLFEE, CMs, PM, and SD was performed to predict the possible interaction between PLFEE and CMs, using an ATR-FTIR spectrophotometer (Bruker Alpha II, Bruker Optics, Ettlingen, Germany). Data were acquired using OPUS software (OPUS software version 7.0). Each spectrum was recorded from 4000 to 400 cm^{-1} with 4 cm^{-1} spectral resolution and 40 spectral scans.

High-performance thin layer chromatography

The compatibility of PLFEE with the formulation excipients was further verified by HPTLC analysis. The integrity of PIP and PLGN in the PLFEE, PM, and SD was investigated by qualitative fingerprinting analysis with the HPTLC instrument (CAMAG, Switzerland) equipped with WinCATS software (Version: 1.4.7.2018). Analysis was carried out on 20 × 10 cm silica gel 60 F254 pre-coated aluminum plates (E. Merck, Darmstadt, Germany). The pure PIP, PLGN, PLFEE, PM, and SD formulations were dissolved in ethanol, centrifuged, and the supernatant was collected for HPTLC analysis. Accurately 5 µL of each sample was applied (dosage speed was 100 nL/s in triplicate with a bandwidth of 8 mm by Linomat V sample applicator (CAMAG, Switzerland) fitted with 100 µL CAMAG syringe at an initial distance of 15 mm from the left side and 8 mm from the bottom of the pre-coated aluminum plate. Out of various reported mobile phase systems, toluene:ethyl acetate (6:4 v/v) was selected due to its better band resolving capacity and higher resolution. After sample application, the plate was developed in a pre-saturated twin trough glass chamber (CAMAG, 20 × 10 cm) up to 90 mm distance using 20 mL of the mobile phase. The developed plate was dried by hair drier (Philips, India); the slit dimension was positioned at 6.00 × 0.45 mm micro and scanned by HPTLC scanner (CAMAG TLC Scanner IV) at a scanning speed of 20 mm/s at 340 and 342 nm. The retardation factor (R_f) values of the bands of the samples and pure phytoconstituents were compared to determine the drug-excipient compatibility [47]. The fingerprint of the developed plate was observed in CAMAG TLC Visualizer 2, and photographs were captured by the embedded charge-coupled device (CCD) camera (SONY, Super HAD, HDR).

Contact angle

Contact angle (θ) of PLFEE and SD was measured via image analysis method utilizing sessile-drop goniometry with the help of a calibrated drop shape analyzer (DSA25S, KRÜSS GmbH, Hamburg, Germany) equipped with a digital camera (ALLIED Vision Technologies, Stadtroda, Germany) and KRUSS advance software (1.6.2.0). The equipment was calibrated (object size 0.5 mm and magnification factor 141.2 Px/mm) before the measurements and analysis was performed at 20 °C. The thin dried films of samples were prepared by spreading the PLFEE or SD methanolic solution (0.5 g/mL) uniformly on microscope slides in an area of 4 cm^2 and allowing the solvent to evaporate in a vacuum oven at 40 °C to produce a uniform film. Water was loaded in 1 mL of a disposable syringe, and 2 µL was dropped at a rate of 2.666 µL/s on the plain film of PLFEE or optimized SD on a microscope slide. The digital images of the drop were captured by a camera, and the image of the water drop was

processed by KRUSS advance software to obtain the contact angle. A minimum of 10 images of each drop were captured to obtain the left contact angle (θ_L), right contact angle (θ_R), and mean contact angle (θ_M). The experiment was carried out in triplicate, and the average was reported.

High-resolution scanning electron microscopy

Representative HRSEM photomicrographs of PLFEE, CMs, PM, and optimized SD were captured using a high-resolution scanning electron microscope (FEI Nova™ Nano SEM 450, FEI, USA) equipped with Everhart–Thornley detector (ETD) and xT Microscope control software (version 1.0) at a voltage of 15 kV. Further, to study the crystal property, samples (PIP, PLFEE, and SD) were solubilized in methanol, dropped on a glass slide, and dried overnight, and the produced films were subjected to HRSEM analysis. The samples were prepared by mounting on aluminum stubs using double-sided carbon tape followed by sputter coating by a desk sputter coater (DSR 1, Nanostructured Coating Co., Iran) with gold and palladium (at a ratio of 60:40 w/w) for 120 s.

Polarized light microscopy

PLM of PLFEE, CMs, PM, and the SD was performed at 10X magnification using a polarizing microscope (Radical RXLr-5, New Delhi, India) equipped with a digital camera (5 MP, Microscopic Procam Camera) and Radical ProCam software (version 3.7) under the crossed polarizer analyzer arrangement at room temperature. Samples were sprinkled on a microscopic glass slide and examined at various angles by rotating the analyzer slider fitted at the top. The microscopic analysis was carried out in triplicate to validate the experimental outcomes.

Moisture content analysis

The moisture content of SD was evaluated by a moisture analyzer (AXIS, Poland) at 70 °C using a halogen radiator for a short duration (30 s). The moisture content was determined in triplicate, and the average was reported.

In vitro dissolution, release kinetics

In vitro dissolution was performed using a USP Type-I dissolution apparatus (Electrolab Trust-E08, Mumbai, India), at 37 ± 0.5 °C with basket rotation of 100 rpm, using 900 mL of 0.1 N HCl (pH: 1.2) as dissolution media. Accurately 50 mg standardized PLFEE (equivalent to 18.85 mg of PIP), an equivalent amount of PM, and optimized SD were encapsulated in empty hard gelatin capsules (Size 00) and used for dissolution study. At predetermined time intervals (i.e., 0.083, 0.25, 0.5, 0.75, 1, 1.5, 2, 2.5, 3, 4, 5, 6, 8, 10, 12, 14, 16, 18, 20, 22, and 24 h), 2 mL of aliquots of medium was withdrawn and replenished with an equal volume of fresh media for maintaining sink condition. The withdrawn samples were centrifuged (10,000 rpm for 15 min) and filtered (0.45 µm PVDF membrane filter), re-extracted to HPLC grade methanol, and quantified for PIP content by the validated HPLC method. The analysis was executed in triplicate, and the average cumulative % of drug released was plotted against time to study the pattern of release.

The mathematical model-dependent method was utilized to know the release kinetics of PIP from the SD. The data of in vitro dissolution were fitted to different kinetic models (first-order, zero-order, Korsmeyer-Peppas, Hixson-Crowell cube-root model, and Higuchi model) by using regression analysis to evaluate the release kinetics of PIP. The linear regression analysis was carried out, and the coefficient of correlation (R^2) in each case was determined [48]. Furthermore, to understand the mechanism of PIP release from the SD, the first 60% of the release data were fitted to the Korsmeyer-Peppas model (Eq. 12).

The following models are considered.

$$Zero-order\ kenetics,\ C_0 - C_t = K_0 t \tag{9}$$

where C_0 is the initial drug concentration at zero time ($t=0$), C_t is the quantity of drug released at time t, and K_0 is the zero-order release constant.

$$First-order\ kenetics, \mathrm{Log}C = \mathrm{Log}C_0 - \frac{K_1 t}{2.303} \tag{10}$$

where C is the percent of drug remaining at time t, C_0 is the initial concentration of the drug, and K_1 is the first-order rate constant.

$$Higuci, Q = K_H t^{1/2} \tag{11}$$

where Q is the amount of drug released in time t, and K_H is the Higuchi dissolution constant.

$$Korsmeyer-Peppas, \frac{M_t}{M_\infty} = k_{kp} t^n \tag{12}$$

where M_t is the amount of drug released in time t, M_∞ is the amount of drug released after time ∞, M_t/M_∞ is the fraction of drug released at time t, k_{kp} is the Korsmeyer release rate constant, and n is the drug release exponent or diffusional exponent.

$$Hixson-crowel, \sqrt[3]{W_0} - \sqrt[3]{W_t} = K_{HC} t \tag{13}$$

where W_0 is the quantity of drug remaining at time 0 (initial quantity of the drug), W_t is the quantity of drug remaining to be released at time t, and K_{HC} is the Hixson-Crowell rate constant.

Hydrodynamic particle size, size distribution, and zeta potential of the SD in dissolution media

The hydrodynamic size (Z_{avg}), polydispersity index (PDI), and zeta potential (ζ) were estimated to investigate the size, homogeneity, and electrokinetic potential of the particles produced during the dissolution of SD in dissolution media (pH 1.2). During the dissolution study, 500 µL of aliquot was withdrawn from the dissolution vessel after 1 h and diluted 10 times with HPLC grade water, and filtered through a 0.2-µm syringe filter. The Z_{avg}, PDI, and ζ were measured by dynamic light scattering (DLS) [49] using a particle size analyzer (Zetasizer Pro, Malvern Panalytical Ltd., UK) equipped with ZS Xplorer software (version 2.3.1). The Z_{avg} and PDI were measured at 25 °C with a refractive index of 1.333 using DTS 0012 polystyrene disposable cuvette at a backscatter angle of 173°, whereas the zeta potential was evaluated using ZEN1002 universal dip cell having palladium electrodes with 2 mm spacing. The experiments were carried out in triplicate, and the average was reported.

High-resolution transmission electron microscopy (HRTEM) and selected area electron diffraction (SAED) analysis

The HRTEM and SAED analysis of the dissolution sample was carried out to investigate their particulate morphology and crystallinity. The analysis was performed using a high-resolution transmission electron microscope (FEI, TECNAI G2 F20 TWIN, USA) equipped with a high-angle annular dark field (HAADF) detector and Gatan's Digital Micrograph software (version 3.7.4) at 200 kV using a carbon-coated copper grid (400 Mesh, 3.05 mm diameter, Ted Pella). The aliquot ($n=3$) from dissolution was diluted two times with HPLC grade water, filtered through a 0.2-µm syringe filter, and 20 µL was dropped onto the TEM grid and dried overnight at room temperature. The TEM photomicrographs were analyzed by ImageJ software (National Institutes of Health (NIH), Bethesda, MD), version 1.53e, Java 1.8.0_172), a minimum of 17 micelles were measured, and the average size was calculated.

Stability study

The optimized SD ($n=3$) was filled in hard gelatin capsules (Size 00), sealed in double aluminum foil, and exposed to different stability conditions, such as accelerated stability (40 ± 2 °C and 75 ± 5% RH), intermediate stability (30 ± 2 °C and 65 ± 5% RH), and long-term stability (25 ± 2 °C and 60 ± 5% RH). The accelerated and intermediate stability study was carried out for up to 6 months by sampling at 0, 3, and 6 months, whereas the long-term stability study was carried out for up to 1 year by sampling at 0, 3, 6, 9, and 12 months. The stability in each environmental condition was evaluated in terms of appearance, drug content, saturation solubility, crystallinity, thermal behavior, and chemical composition (by functional groups). The drug content and saturation solubility of the optimized formulation were estimated by the validated HPLC. The changes in crystallinity were assessed by XRD and DSC. The changes in thermal behavior were investigated by DSC and TGA analysis. Moreover, the alteration in the important functional groups was investigated through ATR-FTIR spectroscopy.

In vitro cytotoxicity assay

The MTT assay was performed against the melanoma cell line (B16F10) and human embryonic kidney 293 cells (HEK 293) as per our reported method with certain modifications [50]. The cytotoxicity of the optimized SDs was evaluated and compared with PLFEE suspension (simple dispersion in media) and PLFEE solution (dissolved in 0.2% DMSO). The B16F10 and HEK 293 cell lines were obtained from the National Centre for Cell Science (NCCS), Pune, India. The cells were seeded at a concentration of 1×10^6 cells/well in a microtiter plate containing DMEM/F-12 medium with 10% FBS, 50 unit/mL penicillin, and streptomycin and incubated in a 5% CO_2 atmosphere for 24 h at 37 °C to attain 70% of confluency. After the attainment of confluency, the medium was discarded, washed thrice with phosphate-buffered saline (PBS, 10 mM, pH 7.4), and further incubated with serum-free fresh media containing various concentrations (20–200 µg/mL) of test substances (optimized SDs, PLFEE suspension, and PLFEE solution) and negative control (placebo of optimized SDs and 0.2% DMSO) for 24 h. A standard anticancer drug, DTIC (2.5–80 µg/mL), was used as a positive control. The SDs were immediately dispersed in culture media before treatment. Due to the hydrophobic nature of PLFEE, it was solubilized in 0.2% DMSO for treatments. Also, the suspension of PLFEE was made by simple dispersion with the media for comparison purposes. Then, the sample solutions were substituted with serum-free media containing 200 µL of MTT solution (5 mg/mL), and cells were further incubated for 4 h at 37 °C. The previous medium was removed, and the cells were washed thrice with PBS. The formazan crystals generated from MTT reduction by viable cells were dissolved by the addition of 150 µL of DMSO. Then, the absorbance of the solution was measured at 570 nm in a microtiter plate reader (Bio-Rad Laboratories, Munchen, Germany). The percentage cell viability was calculated using the formula in Eq. (14). The experiments were repeated in triplicate, and the average value was reported.

$$\%\ cell\ viability = \frac{Abs_{(t)}}{Abs_{(C)}} \times 100 \tag{14}$$

where $Abs_{(t)}$ and $Abs_{(c)}$ are the absorbances of the plate with the treated sample and the absorbance of the control (without any treatment), respectively. The concentration required for 50% inhibition of cell viability (IC_{50} value) was estimated using non-linear regression analysis of log (concentration) vs. response data by GraphPad Prism 5 Software (GraphPad Software, Inc., San Diego, CA). The obtained average IC_{50} values of 3 experiments of each sample were compared statistically using one-way analysis of variance (ANOVA) followed by Tukey's test. The statistical significance was considered at $p < 0.05$.

Animal studies

The animal experiment was carried out following the approved protocol from Institutional Animal Ethics Committee (IAEC Approval Number: IIT(BHU)/IAEC/2022/001 and IIT(BHU)/IAEC/2023/056). The "Committee for the Purpose of Control and Supervision of Experiments on Animals" (CPCSEA) guidelines were followed for the care and experimentation on laboratory animals. The animals (female Sprague–Dawley (SD) rats: 12–13 weeks old, 280 ± 18.345 g and female C57BL/6 mice: 7–8 weeks old, 18 ± 1.784 g body weight) were housed in cages with open access to water and standard food (Laboratory animal feeds, VRK Nutritional Solutions, Maharashtra, India), maintained in a room at 25 ± 1 °C, 55 ± 5% RH with 12 h of dark/light cycle, and acclimatized to the laboratory environment over 1 week before experiments.

In vivo oral bioavailability study

Female SD rats ($n = 15$), weighing 286 ± 20.531 g, were randomly divided into three groups (5 rats/group), a standardized PLFEE group, PM group, and SD group. Before oral dosing, they fasted for 12 h with free access to water. Samples (PLFEE, PM, and SD) were suspended in 1 mL of 0.5% w/v of sodium carboxymethylcellulose (Na-CMC), mixed by vortex mixture, and used immediately for dosing. A single dose (166.67 mg/kg) of standardized PLFEE (equivalent to 62.83 mg/kg of PIP), an equivalent amount of PM, and SD were administered to rats by oral gavage (stainless steel, Gauge 14). After dosing, 250 µL of blood samples was withdrawn from retro-orbital plexus at 0.25, 0.5, 1, 2, 4, 6, 8, 12, and 24 h and immediately transferred into pre-heparinized (40 IU/mL blood) micro-centrifuge tubes (Eppendorf AG, Hamburg, Germany). Collected blood samples were centrifuged at 10,000 rpm for 10 min, at refrigerated condition (4 °C) to separate plasma, and supernatant plasma samples were stored at − 20 °C until analysis. Accurately 100 µL of each plasma sample was mixed with 10 µL (100 µg/mL) of p-dimethylaminobenzaldehyde (p-DMAB) as internal standard (IS) in a 1.5-mL of micro-centrifuge tube. Then, the plasma protein precipitation and extraction of PIP and IS were carried out by adding 0.890 mL of HPLC grade methanol, followed by vertexing vigorously for 5 min and sonicating for 10 min at 40 kHz ultrasonic frequency for maximum extraction. The samples were centrifuged at 10,000 rpm for 10 min at 4 °C, and the supernatant was filtered through a 0.22-µm PVDF membrane filter to obtain a clear organic layer. Then, the organic layer was evaporated in a vacuum under a gentle stream of nitrogen, reconstituted with 1 mL of HPLC grade methanol, filtered through 0.22-µm PVDF membrane filter, and kept in 1.5 mL of screw top amber–colored autosampler HPLC vials (Agilent, USA), before the HPLC analysis. The detailed HPLC methodology for the estimation of PIP in rat plasma with complete validation is provided in the supplementary file (Section 1.5). The PK parameters of SD were estimated through PK Solver software (version 2.0) [51] and compared with PM and PLFEE. Maximum plasma concentration (C_{max}), time to reach maximum concentration (T_{max}), the area under the curve ($AUC_{0–24\,h}$ or $AUC_{0-\infty}$), elimination half-life ($t_{1/2}$), and mean residence time (MRT) were obtained by non-compartmental analysis based on plasma drug concentration–time curve. The relative bioavailabilities (F_{rel}) of SD (test) to that of neat PLFEE (Reference 1) or PM (Reference 2) were calculated using Eq. (15).

$$F_{rel} = \frac{AUC_{test}}{AUC_{Reference}} \times 100 \tag{15}$$

Acute oral toxicity study (LD50) and in vivo anticancer activity in melanoma (B16F10)–bearing C57BL/6 mice

Acute oral toxicity was carried out using healthy nulliparous and non-pregnant female C57BL/6 mice as per Organization for Economic Co-operation and Development (OECD) guidelines 425 using up-and-down-procedure (UDP) [52]. The detailed methodology for the acute oral toxicity study has been described in a supplementary file (Section 1.6). The in vivo anticancer activity of standardized PLFEE, SD, standard marketed drug (dacarbazine) was evaluated against B16F10 melanoma–bearing C57BL/6 female mice. The animals were kept in cages, with free access to food and water, and kept under controlled environmental conditions on a 12-h dark/light cycle in a room at 25 ± 1 °C and 55 ± 5% RH. Before tumor induction, the hair at the dorsal side was carefully removed with an electric clipper. The B16F10 murine melanoma cell line was procured from the National Center for Cell Science (NCCS, Pune, India). The cell line was grown in DMEM/F-12 media supplemented with 10% fetal bovine serum (FBS) and antibiotics (streptomycin-penicillin solution, 50 unit/mL) at 37 °C in a humidified atmosphere containing 5% CO_2. The cells were

cultured up to 90% confluency in T75 Flasks and harvested for in vivo study by trypsinization followed by centrifugation (5000 rpm), washing, and pellet dispersion in phosphate-buffered saline (PBS, pH 7.4). The syngeneic transplantation model was used to develop a solid tumor in C57BL/6 mice. For in vivo experiments, the harvested cells were adjusted to 1×10^6 cells/0.1 mL in PBS, and accurately 100 µL of the cell suspension was subcutaneously injected into C57BL/6 mice. After 7 to 8 days of injection, mice bearing palpable tumors (volume: 35 ± 3 mm^3) were grouped into seven groups ($n = 5$) as per the experimental design. Standardized PLFEE (200 mg/kg b.wt, based on preliminary study) or an equivalent amount of optimized SD (with 0.5% Na-CMC) were administered orally (p.o.) by gavage daily up to 30 days. Standard anticancer drug dacarbazine (DTIC) was injected at a dose of 5 mg/kg intraperitoneally (i.p.) after every 2 days up to 30 days [53]. Tumor volume and body weight were measured every alternate day throughout the treatment period.

Experimental design A total of 35 adult female C57BL/6 mice (after 1 week of initial acclimatization and 7-8 days of tumor induction: weighing 21 ± 1.753 g, 9-10 weeks old) were divided into 7 groups as follows:

Group I (Normal control): Non-tumor-bearing mice, receiving vehicle (0.5% Na-CMC) at a dose of 10 mL/kg body weight (b. wt.) p.o. daily.
Group II (Tumor control): Tumor-bearing mice, receiving vehicle (0.5% Na-CMC) at a dose of 10 mL/kg b. wt. p.o. daily.
Group III (Standard drug/DTIC group): Tumor-bearing mice, receiving DTIC (5 mg/kg b.wt.) i.p. every 2 days.
Group IV (PLFEE group): Tumor-bearing mice, receiving standardized PLFEE (200 mg/kg b.wt.) p.o. daily.
Group V (Optimized SD group): Tumor-bearing mice, receiving optimized SD (equivalent to 200 mg of PLFEE per kg b.wt.) p.o. daily.
Group VI (DTIC + PLFEE group): Tumor-bearing mice, receiving standardized PLFEE (200 mg/kg b.wt.) p.o. daily, and DTIC (5 mg/kg b.wt.) i.p. every 2 days.
Group VII (DTIC + SD group): Tumor-bearing mice, receiving SD (equivalent to 200 mg of PLFEE per kg b.wt.) p.o. daily, and DTIC (5 mg/kg b.wt) i.p. every 2 days.

Tumor regression studies The tumor regression studies were carried out as per the reported protocol [14].

Tumor volume (TV) The size of the solid tumor was measured during the treatment using digital Vernier calipers (ZHART, CT-ZT-VERNIER, India), and the tumor volume was estimated by using Eq. (16).

$$TV = \frac{length \times width^2}{2} \tag{16}$$

Volume doubling time (VDT) It is the time required for the solid tumor to achieve double the initial volume.

Tumor growth inhibition (% TGI).
It was estimated at the end of the study using Eq. (17).

$$\%TGI = \frac{1 - (\frac{T_t}{T_0} \times \frac{C_0}{C_t})}{1 - \frac{C_0}{C_t}} \times 100 \tag{17}$$

where T_t and T_0 are the median tumor volume of treated at time t and time 0, respectively. C_t and C_0 are the median tumor volume of control at time t and time 0, respectively. Tumor growth inhibition greater than 50% is considered meaningful.

Tumor weight and histopathology At the end of the study, 5 mice from each group were sacrificed by cervical dislocation for tumor weight and histopathology studies. Tumors from each group ($n = 5$) were collected, weighed, fixed in 10% buffered formalin for 12 h, and similarly processed for histopathology as described in the acute toxicity study [14].

Statistical analysis

The mean and standard deviation (SD) for all experiments were calculated and expressed as mean ± SD. Statistical analysis was performed by one-way ANOVA followed by Tukey's test (for 3 groups or more) or Student's t-test (between two groups) at $p < 0.05$ using GraphPad Prism 5 (GraphPad Software, Inc., San Diego, California).

Results and discussion

Authentication and extraction of fruits

The taxonomical authentication of fruits assured the identity of the received sample as fruits of *P. longum* Linn. (Family: Piperaceae). The detailed interpretation of molecular authentication and BLAST analysis of fruits is shown in the supplementary file (Section 2.1, Fig. S1, Tables S1 and S2). The BLAST analysis results of the rbcL sequence showed a percentage identity of 100% to *P. longum* (Accession: ON720789.1) further confirming the authenticity of the collected fruits. Various steps involved in the extraction of *P. longum* fruits via cold maceration have been schematically represented in Fig. S2. Microwave irradiation was utilized to enhance the yield of extraction. During microwave exposure to crude drugs, volatile substances and moisture evaporate within the cells,

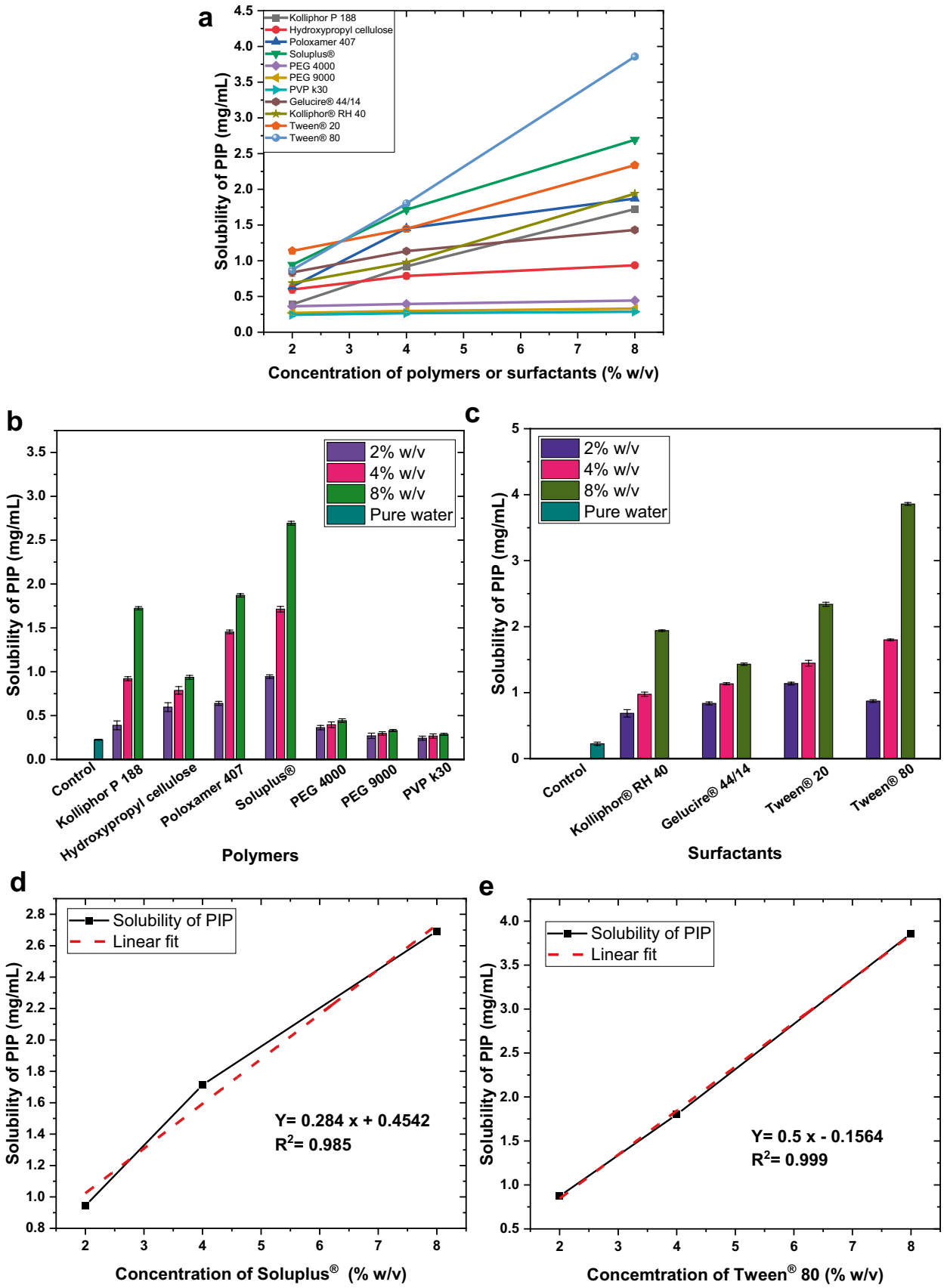
a
Kolliphor P 188
Hydroxypropyl cellulose
Poloxamer 407
Soluplus®
PEG 4000
PEG 9000
PVP k30
Gelucire® 44/14
Kolliphor® RH 40
Tween® 20
Tween® 80
Solubility of PIP (mg/mL)
Concentration of polymers or surfactants (% w/v)
b
2% w/v
4% w/v
8% w/v
Pure water
Solubility of PIP (mg/mL)
Control
Kolliphor P 188
Hydroxypropyl cellulose
Poloxamer 407
Soluplus®
PEG 4000
PEG 9000
PVP k30
Polymers
c
2% w/v
4% w/v
8% w/v
Pure water
Solubility of PIP (mg/mL)
Control
Kolliphor® RH 40
Gelucire® 44/14
Tween® 20
Tween® 80
Surfactants
d
Solubility of PIP
Linear fit
Y= 0.284 x + 0.4542
R2= 0.985
Solubility of PIP (mg/mL)
Concentration of Soluplus® (% w/v)
e
Solubility of PIP
Linear fit
Y= 0.5 x - 0.1564
R2= 0.999
Solubility of PIP (mg/mL)
Concemtration of Tween® 80 (% w/v)

◂**Fig. 1** Phase solubility of PIP from *Piper longum* fruits ethanolic extract (PLFEE) in various carrier matrixes (CMs); **a** solubility of PIP in polymers and surfactants, **b** solubility in polymers, **c** solubility in surfactants, **d** A_N type phase diagram of Soluplus®, and **e** A_L type phase diagram of Tween.® 80. Each value represents the solubility of PIP in 2, 4, and 8% (w/v) aqueous solution of carriers and is represented as mean ± S.D. ($n = 3$)

accumulating and generating a large pressure gradient across the cell membrane. The accumulation of coalesced bubbles causes swelling of cellular structure. With the progression of this event and the increase of the internal pressure, the inside pressure exceeds the mechanical resistance of the cell and causes cellular disruption. The rupture of the cell wall eliminates cellular resistance, facilitates the diffusion of the organic solvent into the cell, and transfers the solubilized phytochemicals into the extraction medium [54]. During the addition of organic solvent to the microwave exposure crude drugs, the organic solvent easily invades the cell, dissolves selected compounds, and then diffuses back into the bulk of the solvent. To avoid the toxicity issues of extracting solvents, it is of utmost essential to use non-toxic or less-toxic solvents and to remove the solvent up to the extent possible [55, 56]. The yield of the obtained dark brown colored extract (PLFEE) was found to be 16.532%. The GC-HS chromatogram of PLFEE (Fig. S3, supplementary file Section 2.3) showed no peak of ethanol, reflecting the ethanol content in the extract is below the detection and quantification limit (LOD = 3.253 ppm, LOQ = 9.859 ppm). As per the ICH Q3C(R8) guideline (guideline for residual solvents), the residual solvents should not exceed recommended levels except in exceptional circumstances. Class 3 solvents (e.g., ethanol, ethyl acetate, acetic acid, acetone) are regarded as less toxic and of lower risk to human health than Class 1 (e.g., carbon tetrachloride, 1,2-Dichloroethane) and Class 2 (e.g., acetonitrile, chlorobenzene, chloroform, cyclohexane) residual solvents. The amounts of Class 3 residual solvents of 50 mg per day or less (corresponding to 5000 ppm) would be acceptable without justification [57].

Validation of HPLC and marker-based standardization of PLFEE

The detailed validation results of the HPLC method are available in the supplementary file (Section 2.4, Fig. S4-S7, Table S3-S9). The overall results of validation reflected the suitability of the HPLC method for quantitative analysis of PIP and PLGN from their respective calibration curves. As herbal drugs are complex mixtures of phytoconstituents, sufficient efforts are needed to guarantee a constant and adequate quality [58]. So, it is very important to standardize the plant extract in terms of chemical markers. Chemical markers (either active markers or analytical markers) refer to phytoconstituents, including primary and secondary metabolites and other macromolecules [58]. The amount of a chemical marker is a signifier of the quality of an herbal product. Standardization ensures that each dosage unit of the herbal product will deliver the same amount of phytoconstituents, which is a prerequisite for reproducible therapeutic effects. The detailed results of marker-based standardization of PLFEE by the validated HPLC method have been described in the supplementary file (Section 2.5, Fig. S8). The quantity of PIP and PLGN was found to be 377.0687 ± 1.453 mg and 6.72 ± 0.108 mg/g of dried PLFEE, respectively.

Phase solubility study

Various hydrophilic polymers and surfactants were screened out by phase solubility study to select the most suitable carrier matrix for the preparation of SD. The solubility results of PIP (in PLFEE) tested in 2, 4, and 8% w/v aqueous solution of each CMs are shown in Fig. 1a–e. The solubility values depend on the slope values of the plot of CM concentrations v/s solubility. The higher the slope value, the superior the solubilization power of that CM (Fig. 1a, Table S10) [59]. The Soluplus® showed the highest slope value (0.284) among the polymers, and Tween® 80 showed the highest slope value (0.5) among the surfactants, signifying the best capacity to solubilize PIP. Thus, among the polymers, the Soluplus® showed the highest PIP solubility (Fig. 1b), and among the surfactants, the Tween® 80 showed the highest PIP solubility (Fig. 1c). Other polymers and surfactants also showed a considerable rise in the solubility of PIP than the solubility in pure water. In most of the cases, the solubility was found to be improved with a rise in the concentration of polymers or surfactants. Similar results have been testified for many poorly soluble drugs/phytoconstituents using hydrophilic carriers due to the formation of water-soluble complexes between the drug and the CMs [46, 59–61]. The estimated Gibbs free energy transfer (ΔG_t°) values, obtained from the phase solubility study, which is a critical thermodynamic factor associated with the solubility of PIP or PIP with polymeric/surfactant aqueous solution are presented in Table S10. Change in ΔG_t° values is an indication of the change in solubility from PIP to PIP-polymeric or surfactant solution [40]. All the obtained ΔG_t° values were found to be negative. The negative values of ΔG_t° reflect the spontaneous solubilization of PIP in those aqueous polymeric or surfactant solutions, and the solubilization process is energetically favorable [39, 40]. The lowest ΔG_t° values are obtained with the highest polymer or surfactant concentrations. This revealed that the solubilization process is more favorable at higher polymeric or surfactant concentrations [39–41].

Phase solubility study in Soluplus® displayed an improvement in solubility of PIP with increasing the concentration of polymer, with r^2 value equal to 0.985, giving A_N type of phase diagram (Fig. 1d), where "A" represents the polymer-drug

combination is soluble in media and the subscript "N" represents a negative deviation from linearity [38, 46, 62]. This finding is consistent with previously reported solubility results regarding the increased aqueous solubility of BCS Class II drug carvedilol by Soluplus® with such type of phase diagram [46]. Solubility of PIP in 8% w/v of Soluplus® was found to be 2.693 ± 0.022 mg/mL compared to PIP (PLFEE) in water (0.224 ± 0.005), corresponding to a 12.022-fold increase, demonstrating excellent affinity between PIP and Soluplus®. The increase in solubility can be explained by micellar solubilization [46]. The self-micellization behavior of Soluplus® increases wettability, reduction of the interfacial tension between the drug and the aqueous solution, and ultimately increases the saturation solubility. The micellization of Soluplus® in water was reported to be a spontaneous endothermic process above the critical micelle concentration (CMC) and critical micelle temperature (CMT) in the presence or absence of drug candidates [63]. Soluplus® is a free-flowing white to slightly yellowish triblock graft copolymer comprising polyvinyl caprolactam (57%), polyvinyl acetate (30%), and polyethylene glycol (13%) having a molecular weight ranging from 90,000 to 140,000 g/mol, and HLB value ~ 14.0 [63–65]. The polymer possesses an amphiphilic chemical structure (Fig. S9a), having a massive number of hydroxyl groups that behave as an excellent solubilizer for poorly soluble drugs in water [46]. The PEG acts as the hydrophilic head group, and the polyvinyl acetate with polyvinyl caprolactam acts as the hydrophobic tail of the amphiphile [63, 65]. The hydrophobic part forms the core of the micelle, whereas the hydrophilic group is positioned towards the aqueous medium, which forms the outer part of the micelles (Fig. S9a) [63].

Similarly, the phase solubility study in Tween® 80 presented an increase in PIP solubility with increasing the concentration of surfactant, with r^2 value of 0.999, giving A_L type of phase diagram (Fig. 1e), where "A" represents the polymer-drug combination is soluble in media and the subscript "L" represents the linearity [38, 62]. Solubility of PIP in 8% w/v of Tween® 80 was found to be 3.858 ± 0.023 mg/mL as compared to PIP in PLFEE (0.224 ± 0.005 mg/mL), corresponding to a 17.223-fold increase, indicating excellent affinity between PIP and Tween® 80. Tween® 80 (Polyoxyethylene (20) sorbitan monooleate) is a nonionic surfactant with low cost and low toxicity [66]. The amphiphilic Tween® 80 is comprised of hydrophilic ethylene oxide (20) with sorbitol (1) groups, and the hydrophobic part comprising of oleic fatty acid (1). At concentrations above the CMC, the surfactant monomers aggregate to form micelles to diminish the free energy of the system [66]. The micellar solubilization of hydrophobic candidates by Tween® 80 was schematically represented in Fig. S9b. The amphiphilic nature of Tween® 80 solubilizes the PIP through micellar solubilization in which the hydrophilic head groups are towards the water medium and the hydrophobic tail forms the core of the micelle and are towards the hydrophobic PIP.

Formulation of SD

The best hydrophilic polymer and surfactant, that confirmed the maximum solubility of PIP among the tested CMs, were chosen for the development of SD. The phase solubility result justified the selection of Soluplus® and Tween® 80 as the most appropriate CMs for the development of SD. Various steps involved in the development of PLFEE containing SD and its incorporation into a hard gelatin capsule (size 00) are represented in Fig. 2a. Solvent evaporation by rotatory vacuum evaporation was widely exploited for the development of SD on a lab scale [44, 59, 67–69]. Rotatory vacuum evaporation allows the evaporation of the solvent under reduced pressure at a lower heating temperature, which is suitable for thermolabile drug candidates [68]. Soluplus® was initially established as a pharmaceutical additive for hot-melt extrusion and has been testified in various findings to form amorphous SD [46, 63, 70–73]. The amphiphilic nature of Soluplus® allows it to solubilize in aqueous and organic solvents. Its solubility in volatile organic solvents makes the solvent evaporation method suitable for the formulation of SD [65]. Soluplus® is categorized as a carrier for fourth-generation SD [46]. The nonionic surfactant Tween® 80 is also frequently reported as CM for the development of SDs [60, 61, 74]. The incorporation of surfactants into SD improves the solubility as well as permeability through the gastrointestinal membrane during oral administration. Since Tween® 80 is liquid, which may produce a sticky formulation, the maximum amount of Tween® 80 that can be incorporated into the SD without the development of a sticky product was chosen for the development of SDs. The Soluplus® also possesses surfactant-like behavior, which improves the solubility and permeability of drugs across a biological membrane. Thus, the 4th generation ternary SDs (PLFEE-SDs) were prepared using standardized PLFEE, Soluplus®, and Tween® 80.

Due to limited toxicity and excellent solubilizing ability, ethanol and acetone (Class III solvents) were used for the preparation of SD. Initially, ethanol was used to dissolve PLFEE and CMs for the development of SD. However, a sticky product (Fig. 2b) and/or rubbery rigid film (Fig. 2c) were formed with discontinuous and/or continuous vacuum evaporation. Further, a low volume of ethanol (2 mL) was used to dissolve PLFEE, and acetone (10 mL) was used to solubilize CMs for the development of SD with continuous vacuum evaporation. A white-colored, highly porous, dried, homogeneous thin film of SD was formed (Fig. 2d). Hence, ethanol and acetone were used further for the formulation of PLFEE-loaded SD. Overnight vacuum drying of the SD removed the residual organic solvents. The high volatility of acetone compared to ethanol allowed the rapid

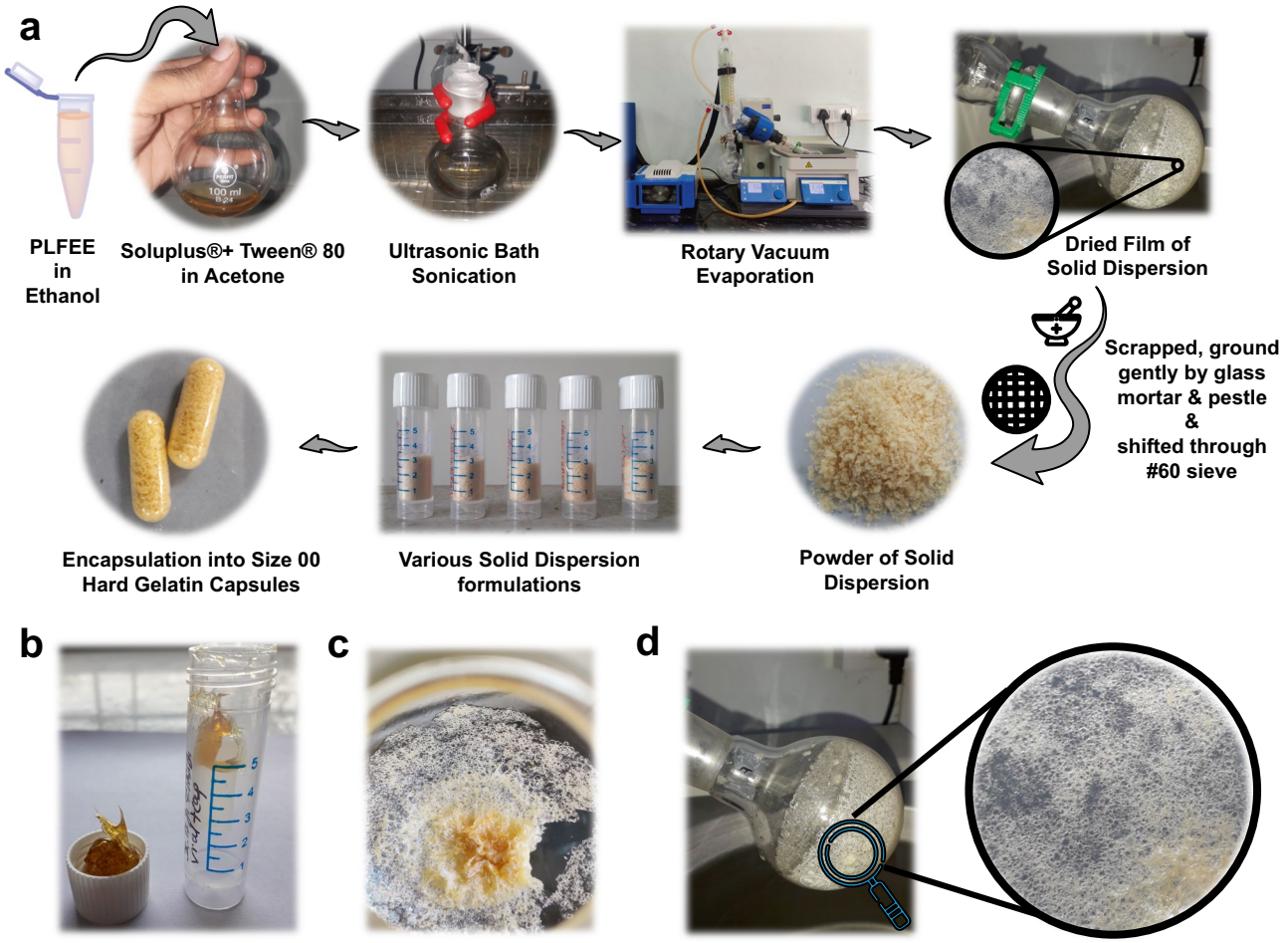

Fig. 2 Formulation development of SDs and formulation consequences. **a** Various steps involved during the development of PLFEE-loaded solid dispersion, **b** sticky product, **c** rubbery film type product, and **d** highly porous dried thin film of formulation

evaporation of the solvent, leading to a porous solid film, which was easily scrapped by a spatula, grounded by mortar and pestle, and shifted through mesh # 60 for obtaining powdered SDs. Rapid solvent evaporation (70 rpm, 50 °C) causes channeling in SDs, increasing the porosity, specific surface area, and ultimately the dissolution rate [26].

Quality by design and optimization

Response surface methodology

RSM in formulation development permits understanding the changes in a particular response (Y) for the changes in the independent variables (X_1, X_2, and X_3). The study of the impact of various factors on the response by the one-factor-at-a-time (OFAT) approach is very time taking, requires considerable amounts of chemical cost, and human efforts. Systematic optimization of the formulation was followed instead of the OFAT approach by employing the quality by design (QbD)–based formulation by design (FbD) as per the ICH Q8 (R2) guideline. In the FbD approach, one can define the quality target product profile (QTPP) and response variable (critical quality attributes (CQAs)) and identify the influence of independent variables (critical material attributes (CMAs) and critical process parameters (CPPs)) on CQAs [75]. A Box-Wilson central composite design (CCD) was employed to generate a second-order polynomial equation for the CQAs in RSM [43]. Compared to face-centered CCDs ($\alpha = 1$), near-rotatable or rotatable CCDs ($\alpha = 1.414$) provides decreased prediction error and improved valuation of curvature (quadratic) effects. Compared to Box-Behnken design (BBD), the CCD offers a wide design space due to the inclusion of axial points, in which the influence of various factors at five different levels on the response can be easily analyzed. The rotatable CCD model was widely explored for response surface analysis and optimization. [44, 76]. Table 1 shows the levels of the evaluated factors (CMAs and CPP) and the CQA. The composition of 20 trial batches with their CQA (saturation solubility of PIP) is shown in Table 2.

Table 1 Coded levels, real values for each factor under experiment, and CQA

Screened factors (CMAs & CPP) and responses (CQAs)	Levels				
	Coded values				
	−1.681	−1	0	+1	+1.681
Independent variables (CMA and CPP)	Real values				
Soluplus®:PLFEE (X_1, w:w)	0.636	2	4	6	7.363
Tween® 80:PLFEE (X_2, w:w)	0.131	0.2	0.3	0.4	0.468
Sonication time (X_3, min)	19.773	30	45	60	70.226
Dependent variables (CQAs)	Goal				
Saturation solubility of PIP (Y, mg/mL)	To maximize				

CQA critical quality attributes, *CMAs* critical material attributes, *CPP* critical process parameter

The statistical model fit summary is represented in Table 3. The higher R^2 values reflect the better significance of the experimental model [41]. The cubic model was found to possess a higher R^2 value (0.991) compared to other models. However, the sequential p-value was found to be high ($p > 0.05$), reflecting the model's insignificance. Hence, the cubic model was found to be aliased. The quadratic model produced the highest adjusted and predicted R^2 values for response (Y) over the liner, 2FI, and cubic models (Table 3). The software suggested the quadratic model as the best-fit model to describe the experimental design based upon a high model R^2 value (0.9854), an acceptable difference (< 0.2) between adjusted and predicted R^2 values, and a high lack of fit value (> 0.05). The R^2 value of 0.9854 in the quadratic model signifies that 98.5% of the data can be explained, analyzed, and examined through this model. From the model summary statistics (Table 3), the quadratic model comes out best since it exhibited low standard deviation ("Std. Dev."), high "R-Squared" values, and a low "Predicted Residual Sum of Squares" (PRESS). Hence, the effect of various variables on the saturation solubility of PIP in SDs can be best explained, analyzed, and interpreted by the quadratic model using the quadratic equation.

Statistical analysis was executed using the analysis of variance (ANOVA) program in the Design-Expert software, and the results are shown in Table 4. At a 95% level of confidence, the overall model p-value (i.e., 0.0001 < 0.05) for Y indicates the significance of the model and a good fit with the statistical results [41]. Except for the term X_2X_3, the p-values for all model terms were found to be < 0.05, reflecting the appropriateness of the model for response surface analysis. In the case of many insignificant model terms, the model

Table 2 Central composite design (CCD)–based trial formulation batches with respective CQA

Batches	Independent variables (CMAs and CPP)						Response/CQA or Y (mg/mL)
	Coded values			Actual values			
	X_1 (w:w)	X_2 (w:w)	X_3 (min)	X_1 (w:w)	X_2 (w:w)	X_3 (min)	
1	+1	+1	−1	6	0.4	30	5.379 ± 0.021
2	0	0	0	4	0.3	45	4.784 ± 0.034
3	0	0	+1.681	4	0.3	70.226	5.196 ± 0.017
4	−1.681	0	0	0.636	0.3	45	3.661 ± 0.012
5	0	+1.681	0	4	0.468	45	5.732 ± 0.123
6	0	−1.681	0	4	0.131	45	4.998 ± 0.032
7	0	0	0	4	0.3	45	4.922 ± 0.033
8	+1	−1	+1	6	0.2	60	5.285 ± 0.031
9	0	0	−1.681	4	0.3	19.773	4.895 ± 0.011
10	0	0	0	4	0.3	45	4.710 ± 0.045
11	−1	−1	−1	2	0.2	30	4.303 ± 0.036
12	−1	+1	+1	2	0.4	60	4.723 ± 0.054
13	−1	−1	+1	2	0.2	60	4.463 ± 0.153
14	0	0	0	4	0.3	45	4.733 ± 0.205
15	−1	+1	−1	2	0.4	30	4.705 ± 0.035
16	+1.681	0	0	7.363	0.3	45	5.169 ± 0.081
17	+1	+1	+1	6	0.4	60	5.828 ± 0.168
18	0	0	0	4	0.3	45	4.703 ± 0.218
19	0	0	0	4	0.3	45	4.733 ± 0.038
20	+1	−1	−1	6	0.2	30	4.728 ± 0.073

Results were represented as mean ± SD ($n = 3$)

Table 3 Results of model fit summary and model summary statistics

Fit summary report						
Source (Models)	R^2 value	Sequential p-value	Lack of fit p-value	Adjusted R^2	Predicted R^2	
Linear	0.718	0.0001	0.0032	0.66514	0.5056	
2FI	0.747	0.6895	0.0021	0.63041	0.5225	
Quadratic	0.985	< 0.0001	0.5444	0.97227	0.9364	Suggested
Cubic	0.991	0.4064	0.5987	0.97415	0.8822	Aliased
Model summary statistics						
Source	Std. Dev	R^2	Adjusted R^2	Predicted R^2	PRESS	
Linear	0.2791	0.7180	0.6651	0.5056	2.1865	
2FI	0.2933	0.7471	0.6304	0.5225	2.1116	
Quadratic	0.0803	0.9854	0.9723	0.9364	0.2812	Suggested
Cubic	0.0775	0.9918	0.9742	0.8823	0.5207	Aliased

2FI two-factor interaction model

reduction approach may improve the model predictability. The single insignificant model term does not greatly affect the model; hence, the model reduction approach was not used in our study. The "Lack of Fit Tests" compares residual error with pure error from replicated design points. The lack of fit p-value (0.5444) was found to be non-significant ($p > 0.05$), which is a primary requirement for such studies. This non-significant lack of fit p-value represents the ability of the model to fit the data properly to the model equation [76]. The adequate precision value represents the signal-to-noise ratio, and a value greater than 4 is necessary [43]. As per the utilized rotatable CCD model, the obtained adequate precision value was found to be 37.2901, reflecting the attainment of adequate precision. Hence, this model can be utilized to explore the design space to find out the optimized SDs formula.

Diagnostic plots (Fig. S10a-f) allow the investigation of the goodness of fit of the proposed model. The linearity in the "normal plot of residual," optimum lambda value in the "Box-Cox plot," linearity in the "actual v/s predicted plot," constant range of residuals in the "externally studentized residual v/s predicted plot," randomly scatter within the control limits in

Table 4 ANOVA for quadratic model and fit statistics

ANOVA						
Source	Sum of squares	df	Mean square	F-value	p-value	
Model	4.3582	9	0.4842	75.03	< 0.0001	Significant
X_1	2.2665	1	2.27	351.20	< 0.0001	
X_2	0.6994	1	0.6995	108.39	< 0.0001	
X_3	0.2095	1	0.2096	32.47	0.0002	
X_1X_2	0.0353	1	0.0354	5.48	0.0413	
X_1X_3	0.0856	1	0.0856	13.27	0.0045	
X_2X_3	0.0077	1	0.0078	1.20	0.2987	
X_1^2	0.2394	1	0.2394	37.10	0.0001	
X_2^2	0.6177	1	0.6178	95.73	< 0.0001	
X_3^2	0.1274	1	0.1274	19.74	0.0012	
Residual	0.0645	10	0.0065			
Lack of fit	0.0305	5	0.0061	0.9004	0.5444	Not significant
Pure error	0.0339	5	0.0068			
Cor total	4.4227	19				
Fit statistics						
Standard deviation (SD)	Mean	C.V (%)	R^2	Adjusted R^2	Predicted R^2	Adequate Precision
0.0803	4.88	1.65	0.9854	0.9723	0.9364	37.2901

X_1 = Soluplus®: PLFEE w/w, X_2 = Tween® 80: PLFEE w/w, X_3 = sonication time

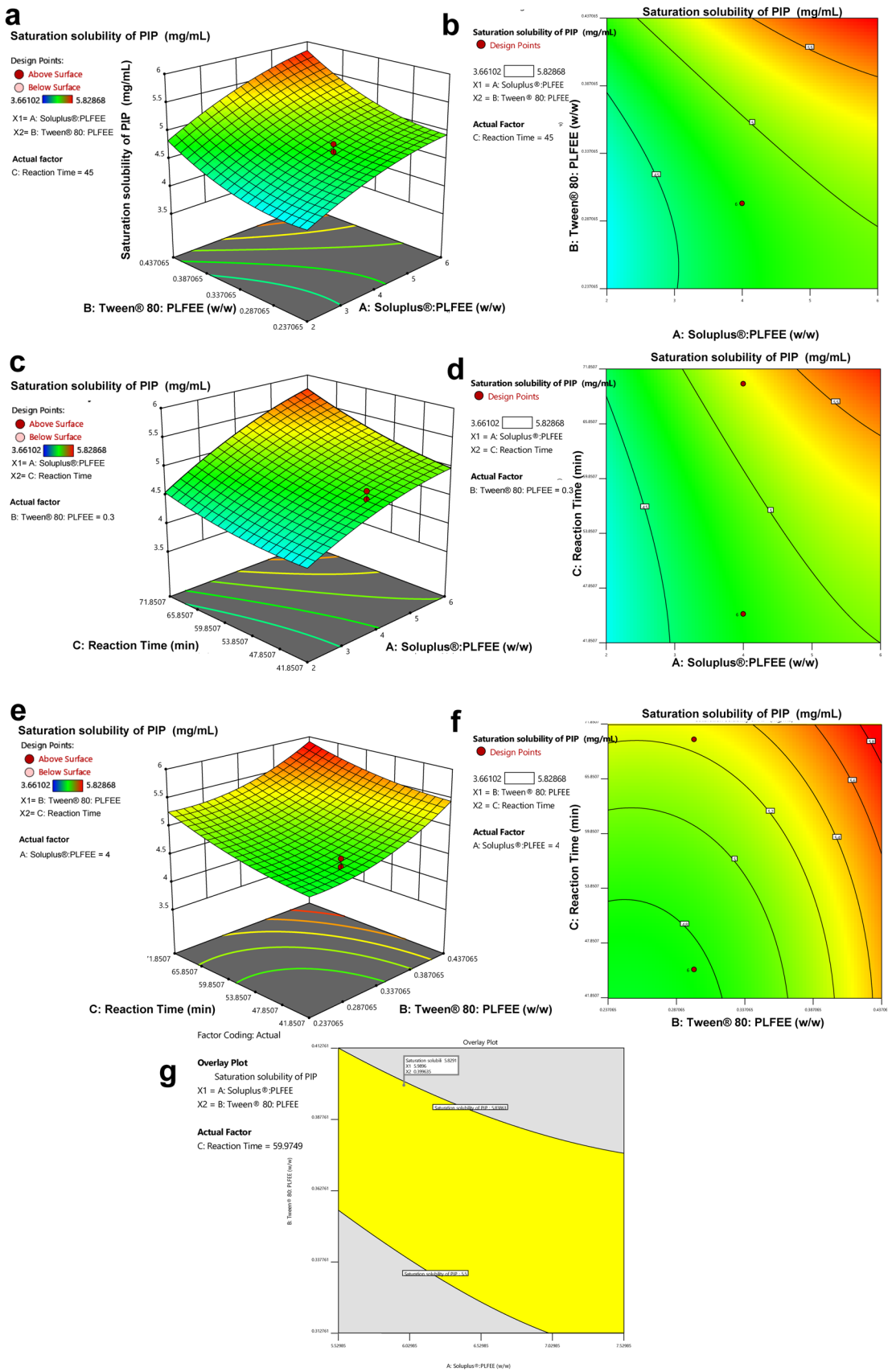
a
Saturation solubility of PIP (mg/mL)
Design Points:
Above Surface
Below Surface
3.66102 5.82868
X1= A: Soluplus®:PLFEE
X2= B: Tween® 80: PLFEE
Actual factor
C: Reaction Time = 45
Saturation solubility of PIP (mg/mL)
B: Tween® 80: PLFEE (w/w)
A: Soluplus®:PLFEE (w/w)
b
Saturation solubility of PIP (mg/mL)
Design Points
3.66102 5.82868
X1 = A: Soluplus®:PLFEE
X2 = B: Tween® 80: PLFEE
Actual Factor
C: Reaction Time = 45
Saturation solubility of PIP (mg/mL)
B: Tween® 80: PLFEE (w/w)
A: Soluplus®:PLFEE (w/w)
c
Saturation solubility of PIP (mg/mL)
Design Points:
Above Surface
Below Surface
3.66102 5.82868
X1= A: Soluplus®:PLFEE
X2= C: Reaction Time
Actual factor
B: Tween® 80: PLFEE = 0.3
Saturation solubility of PIP (mg/mL)
C: Reaction Time (min)
A: Soluplus®:PLFEE (w/w)
d
Saturation solubility of PIP (mg/mL)
Design Points
3.66102 5.82868
X1 = A: Soluplus®:PLFEE
X2 = C: Reaction Time
Actual Factor
B: Tween® 80: PLFEE = 0.3
Saturation solubility of PIP (mg/mL)
C: Reaction Time (min)
A: Soluplus®:PLFEE (w/w)
e
Saturation solubility of PIP (mg/mL)
Design Points:
Above Surface
Below Surface
3.66102 5.82868
X1= B: Tween® 80: PLFEE
X2= C: Reaction Time
Actual factor
A: Soluplus®:PLFEE = 4
Saturation solubility of PIP (mg/mL)
C: Reaction Time (min)
B: Tween® 80: PLFEE (w/w)
Factor Coding: Actual
f
Saturation solubility of PIP (mg/mL)
Design Points
3.66102 5.82868
X1 = B: Tween® 80: PLFEE
X2 = C: Reaction Time
Actual Factor
A: Soluplus®:PLFEE = 4
Saturation solubility of PIP (mg/mL)
C: Reaction Time (min)
B: Tween® 80: PLFEE (w/w)
g
Overlay Plot
Saturation solubility of PIP
X1 = A: Soluplus®:PLFEE
X2 = B: Tween® 80: PLFEE
Actual Factor
C: Reaction Time = 59.9749
Overlay Plot
B: Tween® 80: PLFEE (w/w)
A: Soluplus®:PLFEE (w/w)

◂**Fig. 3** Three-dimensional response surface plots and corresponding counterplots for saturation solubility; **a** and **b** effect of factor X_1 and X_2, considering factor X_3 constant, **c** and **d** effect of factor X_1 and X_3, considering factor X_2 constant, **e** and **f** effect of factor X_3 and X_2, considering factor X_1 constant, and **g** overlay plot as a function of change in X_1 and X_2, considering X_3 constant

the "externally studentized residual v/s run plot," and "residual v/s factor plot" represents the goodness of fit of the proposed model. The projected model polynomial–coded quadratic equation (Eq. 18) was used to make predictions about the response (saturation solubility) for given levels of each factor. This equation identifies the relative impact of the factors by comparing the factor coefficients. The values and signs of the coefficients associated with each factor reflect the magnitude and direction of the effect of the independent variables on response, respectively [41].

Model coded equation

$$\begin{aligned} \textit{Saturation solubility of PIP} = {} & 0.7148 + 0.0611X_1 + 0.0339X_2 + 0.0186X_3 \\ & + 0.0100X_1X_2 + 0.0155X_1X_3 - 0.0047X_2X_3 \\ & - 0.0193X_1^2 + 0.0311X_2^2 + 0.0141X_3^2 \end{aligned} \tag{18}$$

The coefficients with a positive sign demonstrate a positive impact (synergistic effect) on the response (Y), whereas the negative sign demonstrates a negative impact (inverse effect) on the response [41, 43, 44]. The significance of the quadratic polynomial model was assessed by using ANOVA data (Table 4). For any of the terms (main, interaction, or quadratic) in the model, a large "F" value and a small "P" value directed a more significant effect on the response (Y) [43]. The linear variable (X_1) displayed the largest and most significant ($p < 0.05$) effect on the saturation solubility of the SDs, whereas the other two variables (X_2 and X_3) showed slightly lesser effects on Y due to comparatively small "F" value and larger "P" value. Except for X_2X_3, all the interaction terms and the quadratic terms (X_1^2, X_2^2, and X_3^2) displayed a significant effect on Y. The perturbation plot (Fig. S10 g) revealed a steep slope for X_1 compared to other factors (X_2 and X_3), signifying the greater effect of X_1 on the saturation solubility of PIP. The saturation solubility of PIP was found to be increased rapidly when the factor X_1 moved from − 1 to + 1.

The relationship among the factors (X_1, X_2, and X_3) and response (Y) was further inferred from the 3D response surface plots and 2D contour plots (Fig. 3a-f). Increasing the ratio of Soluplus® to PLFEE (X_1) significantly increased the saturation solubility (Y) of PIP ($p < 0.05$). Similar results of increased solubility with an increase in polymer concentrations were previously reported by various authors [41, 46, 77]. The solubility enhancement by Soluplus® can be ascribed to the micellar solubilization behavior of Soluplus® as described under the phase solubility section. The micelle population increased with an increase in the concentration of Soluplus® owing to the improvement of PIP solubility [46]. Similarly, the Y was found to be increased with increasing the Tween® 80 to PLFEE ratio (X_2). The enhanced solubility is attributed to the amphiphilic property of Tween® 80 that solubilize the PIP through micellar solubilization [66]. The higher amount of X_1 and X_2 causes more amorphous modification of the PLFEE and ultimately enhances the saturation solubility. Further, due to the amphiphilic property of both CMs, they reduce the interfacial tension, improve the wettability of PIP in a concentration-dependent manner, and ultimately enhance the saturation solubility. The saturation solubility of PIP was found to be increased with increasing the sonication time. The prolonged sonication time allows better molecular interactions among the PIP (in PLFEE) and CMs (Soluplus® + Tween® 80), causes more amorphous modification, and ultimately enhances the saturation solubility.

Optimization of formulation

The numerical and graphical optimization techniques with the desirability approach were utilized to develop an optimized formulation with the desired responses. The composition of the software-suggested optimized SD was 5.989 w/w of Soluplus®:PLFEE (X_1), 0.399 w/w of Tween® 80:PLFEE (X_2), and 59.974 min sonication time (X_3), which would show saturation solubility of 5.829 mg/mL. The overlay plot as a function of the change in X_1, X_2, at constant X_3 value is shown in Fig. 3g. From the overlay plot, the desired region for constraining variables was identified inside the yellow design space. The flag mark in the yellow zone indicates the optimized batch.

Checkpoint analysis (validation of method)

The experimental and predicted values of Y were 5.672 ± 0.023 ($n = 5$) and 5.829 mg/mL, respectively. The percentage prediction error (% Bias) for the checkpoint batch was found to be − 2.693%, which was < 5% validating the authenticity of predictive capacity and accuracy of the design model [41, 44].

Characterizations of optimized solid dispersion

Drug content and content uniformity

The drug content of SD with respect to PIP ($n = 3$) was found to be 98.079 ± 0.231%. The variation of the PIP content among the sampled specimen from different locations ($n = 3$) of SD powder was found to be very negligible (% RSD < 2%). This indicates the content uniformity of the SD, i.e., the PLFEE is uniformly distributed throughout the CMs

to form amorphous SD without apparent phase separation. Such good content uniformity is ascribed to the molecular level mixing of PLFEE with the CMs in the organic solvent during sonication and rotary-based continuous evaporation during the formulation of SD that will offer dosing uniformity.

Percent yield

The average % yield of SD of 3 independent analyses was found to be 98.231 ± 0.245%. The rotary vacuum evaporation–based method allows the evaporation of organic solvent without loss of formulation as the entire process occurs in a single round bottom flask. Due to the round structure of the flask, a very small quantity of SD remains on its wall, which leads to a slight decrease in the overall yield.

Micromeritics properties

The bulk density and tapped density of SD were found to be 0.283 ± 0.024 g/mL and 0.347 ± 0.025 g/mL, respectively. The angle of repose, CI, and HR values represents the flowability of the powder. The CI of a powder is a measure of bridge strength or potential powder arch and stability, whereas the HR is related to inter-particulate friction [78]. The obtained angle of repose, CI, and HR were found to be 36.623 ± 0.543°, 18.443 ± 0.051%, and 1.226 ± 0.016, respectively, suggesting fair flow property of SD powder [78]. The flow property can be enhanced further by utilizing glidants or lubricants.

X-ray diffraction

XRD is widely used for investigating the molecular order of solid dispersion [26]. The XRD results of standardized PLFEE, Soluplus®, Tween® 80, PM, and optimized SD are shown in Fig. 4a. The PLFEE showed sharp diffraction patterns at 2θ of 12.606°, 14.658°, 19.644°, 21.86°, 24.097°, 25.984°, 31.562°, 37.768°, and 41.231° which is superimposable with the peaks for PIP [79–83], reflecting its crystallinity nature. Soluplus® showed halo diffraction patterns with diffused peaks which are well consistent with reported XRD reports, representing its amorphous nature [46, 72, 84, 85]. Tween® 80 exhibited halo diffractions and diffused peaks, reflecting its amorphous nature. The PM retained the diffraction peaks of PLFEE at 14.811°, 19.88°, 21.976°, 25.751°, and 41.756° with low intensity and broad peaks of CMs, signifying no alteration in the crystallinity of PLFEE. However, the decreased diffraction intensity of PLFEE in PM is due to the higher proportion of Soluplus®. Such results of decreased diffraction intensity of drugs in the presence of a higher proportion of polymers were reported elsewhere [73]. The X-ray diffractogram of the SD presented a typical halo pattern similar to Soluplus® and Tween® 80 with the nonappearance of the characteristic peaks of PLFEE, signifying the completely amorphous form of PLFEE in the SD. The result reflects that the PLFEE is molecularly dispersed in the CMs of SD [86]. Crystalline material possesses strong crystal lattice energy which leads to low aqueous solubility [46]. Therefore, any strategy that outcomes in lower crystal lattice energy or disrupt the crystallinity would improve the water solubility of the drug [46]. SD is an effective formulation strategy to disrupt the crystallinity of the drug partially or totally, resulting in a significant enhancement of solubility. As hydrophilic carriers, Soluplus® and Tween® 80 have been verified to lose the crystallinity of drugs, producing amorphous solid dispersions with improved drug wetting, solubility, and dissolution [46, 60, 61, 68, 72]. In solvent evaporation techniques, after the complete evaporation of the solvent, the drug candidate is ultimately frozen in the carrier matrix without creating a crystal lattice (producing a disordered amorphous state) [68]. The molecular interaction among the PLFEE and CMs (Soluplus® and Tween® 80) could successfully change the crystal form of the PLFEE into an amorphous state.

Differential scanning calorimetry

The DSC study was executed to analyze the thermal behaviors of standardized PLFEE, Soluplus®, PM, and optimized SD (Fig. 4b). The PLFEE exhibited a sharp endothermic peak at 121.059° C, signifying its crystallinity, attributed to the melting of numerous phytoconstituents. Soluplus® exhibited a broad endothermic peak at 69.567 °C corresponding to its glass transition temperature (Tg), representing its amorphous nature [46, 87, 88]. The PM showed both the characteristic endothermic peaks of PLFEE at ~ 121.215 °C and CMs at 68.897 °C. However, the decreased intensity and slightly broader endotherm of PLFEE are due to a higher proportion of CMs (dilution effect). The presence of two distinct endotherms in the PM reveals the phase separation state in which the crystalline PLFEE and amorphous CMs coexist in their original state. In contrast, the thermograms of SD did not display the endothermic peak of PLFEE, signifying a complete transition of crystalline extract into its amorphous state. Similar results have been reported previously [46, 69, 72, 88]. The thermogram of SD displayed a broad endothermic peak at 50.239 °C, which is completely different from PLFEE, Soluplus®, and PM. The Tg of Soluplus® was shifted towards its lower temperature (50.239 °C), indicating an interaction between PLFEE and CMs. Analogous results of solid dispersion using Soluplus® were reported previously [68, 69]. The drug and CMs remain dispersed at a molecular level in an amorphous solid solution, resulting in a conversion to an amorphous product that displays a single Tg [26]. The SD displayed a single Tg, demonstrating

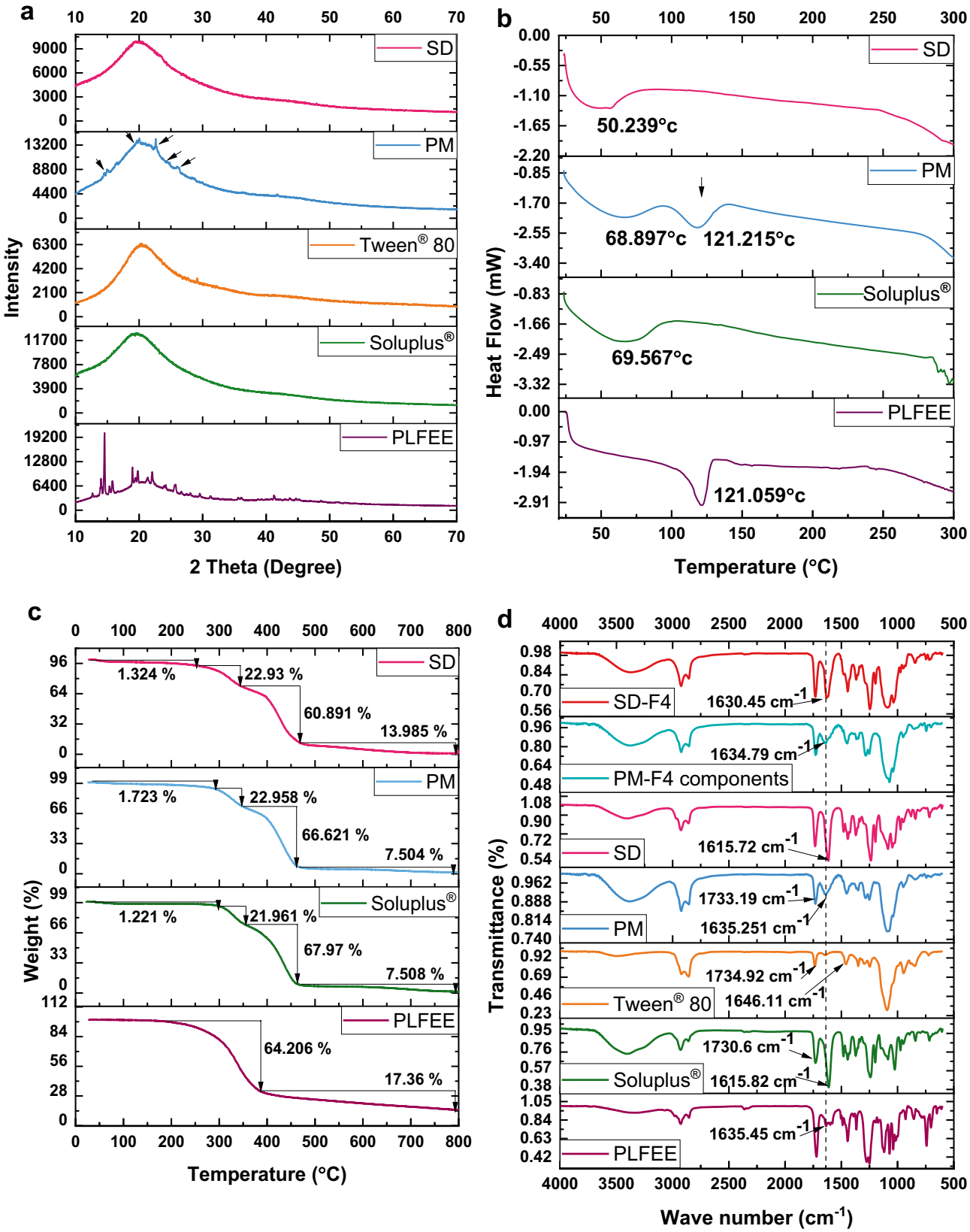

Fig. 4 X-ray diffraction (XRD), differential scanning calorimetry (DSC), thermogravimetric analysis (TGA), and Fourier transform infrared spectroscopy (FTIR) results of solid dispersion formulation and formulation components; **a** XRD diffractograms, **b** DSC thermograms, **c** TGA thermograms, and **d** ATR-FTIR spectra

the amorphous and homogeneous form due to the complete miscibility of the PLFEE in the CMs [26]. The obtained Tg of SD was below the corresponding Tg of polymer and above 40 °C, which was anticipated to be stable when stored at room temperature [69]. According to the Boyer-Beaman rule, a drug candidate that demonstrates good glass-forming possessions has Tg/Tm (in Kelvin) value higher than 0.67 (i.e., as per the rule of $2/3^{rds}$) to produce solid dispersions [84]. Therefore, with a Tg/Tm value of 0.869 K, PLFEE is anticipated to be able to produce solid dispersion.

Thermogravimetric analysis

TGA was carried out to investigate the thermal degradation pattern of formulation components and formulation. The % weight loss of samples during linear heating from 10 to 800 °C is shown in Fig. 4c. The PLFEE displayed two-step degradation patterns, with the initiation of weight loss at ~ 201.978 °C, representing its thermal stability up to this temperature. Further, a significant weight loss of 64.206% from 201.978 to 384.392 °C and 17.36% from 384.392 to 800 °C was noticed. Soluplus® showed a four-step degradation pattern, with the first 1.221% loss of weight at 300.78 °C due to the evaporation of moisture [89]. Apart from this, no potential degradation was observed up to 300.78 °C, demonstrating the thermal stability of Soluplus® up to this temperature. Similar TGA data of Soluplus® was reported previously [89, 90]. Further, a continuous weight loss of 21.961% between 300.78 and 355.183 °C, 67.97% between 355.183 and 464 °C, and 7.508% between 464 and 800 °C was due to its degradation. PM displayed four steps degradation pattern which is almost identical to that of Soluplus® due to its higher proportion. The initial weight loss of 1.723% is ascribed to moisture loss, followed by stepwise weight loss of 22.958% from 294.53 to 347.603 °C, 66.621% from 347.603 to 461.761 °C, and 7.504 from 461.76 to 800 °C. The SD displayed initial weight loss of 1.324% at 205 °C due to moisture loss followed by continuous weight loss of 22.93% from 205 to 344.03 °C, 60.891% from 344.03 to 467.335 °C, and 13.985% from 467.335 to 800 °C. The % weight loss of SD in various steps is different from others, reflecting the existence of an entirely new phase other than PM.

Attenuated total reflectance-Fourier transform infrared spectroscopy

FTIR is a non-destructive vibrational spectroscopic technique for the investigation of the chemical bonds, composition of the drug, and drug-excipient interactions. When various formulation components are mixed at a molecular level, it creates alterations in the oscillating dipole of the molecules. Such alterations are reflected in terms of the frequency, intensity, and bandwidth of the interacting groups [69]. The results of ATR-FTIR are shown in Fig. 4d. The standardized PLFEE showed the aromatic C-H stretching at 2928.865 cm^{-1}, aliphatic C-H stretching of methylenedioxy group at 2855.822 cm^{-1}, carbonyl stretching of -C = O-N = at 1635.45 cm^{-1}, C = C asymmetric stretching of aliphatic diene at 1612.843 cm^{-1}, aromatic C = C stretching of benzene ring 1444.887 cm^{-1}, asymmetrical stretching of = C–O–C at 1246.541 cm^{-1}, symmetrical stretching of = C–O–C at 1036.838 cm^{-1}, C–H bending for trans -CH = CH- at 999.256 cm^{-1}, and C-O stretching of methylenedioxy group at 929.315 cm^{-1}. All the assigned peaks of standardized PLFEE are in accordance with the reported data of PIP due to its relatively higher amount in the extract [26, 91]. The bands at 2928.865 cm^{-1}, 1635.483 cm^{-1}, 1612.843 cm^{-1}, 1444.887 cm^{-1}, and 929.315 cm^{-1} were also contributed by structurally similar constituents like piperlongumine, piperlonguminine, and pellitorine. Peaks at 1720.038 cm^{-1} were ascribed to -C = O stretching of the aldehydic or conjugated ester group. The peak at 1273.941 cm^{-1} was ascribed to aromatic -C-N stretching, 1071.567 cm^{-1} was ascribed to an alcoholic -C-O stretching or -C-N stretch of aliphatic amine or -C-O stretch of ester, or -C–O–C stretch of dialkyl ether group, and peak at 742.544 cm^{-1} was ascribed to bending of the aromatic out-of-plane ring. Soluplus® exhibited a strong broad peak at 3411.878 cm^{-1} (alcoholic -O–H stretching of hydrophilic polyethylene glycol subunits), 2929.03 cm^{-1}, and 2860.94 cm^{-1} (aliphatic -C-H stretching), 1730.609 cm^{-1} (-C = O stretching of the ester group of polyvinyl acetate), 1612.82 cm^{-1} (amidic -C = O stretching of polyvinyl caprolactam), 1443.76 cm^{-1} (-C-H bending), and peaks from 1241.05 to 1025.87 cm^{-1} (-C-O stretching of alcohol or ester or ether groups) [46, 68, 84, 85, 88]. Tween® 80 showed a broad peak at 3506.26 cm^{-1} for an alcoholic -O–H stretching, 2921.93 cm^{-1} for asymmetric stretching of -C-H group, 2857.44 cm^{-1} for the symmetric stretching of the -C-H group, and 1734.92 cm^{-1} for -C = O stretching of ester group [92]. The peak at 1646.11 cm^{-1} was ascribed to C = O stretching of the amide group, and 1456.133 cm^{-1} and 1349.24 cm^{-1} were ascribed to -C-H bending of alkane. Peaks from 1296 to 1093.5 cm^{-1} were ascribed to C-O stretch alcohols, esters, or ethers.

PM showed a strong broad peak at 3378.362 cm^{-1} for an alcoholic -O–H stretching, 2924.278 cm^{-1} and 2857.564 cm^{-1} for aliphatic -C-H stretching, 1733.196 cm^{-1} for -C = O stretching of the ester group, 1636.81 cm^{-1} for carbonyl stretching of the amide group, and 1455.65 cm^{-1} and 1349.92 cm^{-1} for C-H bending of alkane groups, and 1284.765 to 1093.5 cm^{-1} were ascribed to C–O stretch alcohols, esters, or ethers. The FTIR of the physical mixture (PM-F4 components) was recorded to investigate the dilution effect by CMs. A similar FTIR fingerprint was obtained

as that of PM. However, the spectral intensity of PLFEE peaks was found to be increased due to the presence of a lower proportion of CMs in the PM-F4 compared to PM. The spectra of PM and PM-F4 are the superposition of Soluplus®, Tween® 80, and PLFEE, representing the chemical compatibility among the used excipients and standardized plant extract [68].

The SD showed a broad vibrational peak at 3413.43 cm^{-1} for an alcoholic -O–H stretching, 2926.99 cm^{-1} and 2858.85 cm^{-1} for aliphatic -C-H stretching, a sharp peak at 1733.378 cm^{-1} for -C = O stretching of the ester group, 1616.873 cm^{-1} for -C = O stretching of the amide group, 1444.22 cm^{-1} for -C-H bending, and peaks from 1238.94 to 1044.79 cm^{-1} for -C-O stretching of alcohol or ester or ether groups. The characteristic peak of PLFEE at 1636 cm^{-1} was found to be disappeared in SD. The spectra of optimized SD showed the predominance of the characteristic peaks of Soluplus®, which might be due to its higher proportion in the formulation. However, in the case of PM, the characteristic peak of PLFEE at 1636 cm^{-1} was retained even at a higher proportion of CMs, which did not support the disappearance of characteristic peaks of PLFEE in SD due to a higher proportion of CMs. The predominance of the characteristic peaks of Soluplus® and the disappearance of the characteristic peak of PLFEE are possibly due to the molecular level trapping of PLFEE inside the CM matrix of SD [93]. A similar result was also observed with SDs of atorvastatin calcium with Soluplus®, where the spectra of SDs lack characteristics spectrum of atorvastatin calcium and displayed the characteristic peaks of Soluplus® [39]. To elucidate further, the spectra of SD-F4 (containing a lower amount of CMs) were recorded. The intensities of Soluplus® peaks were found to be decreased in SD-F4 due to its lower proportion compared to SD. However, the shifting of characteristic carbonyl stretching (-C = O-N =) band of PLFEE occurred from 1635.66 cm^{-1} to a lower wave number (1630.45 cm^{-1}). The minute shifting of the carbonyl stretching band in formulations may be ascribed to the possible hydrogen bonding between the -C = O of PLFEE and the hydroxyl group of CMs (Soluplus® + Tween® 80). Similar H-bonding between PIP and sorbitol and PEG in the case of solid dispersion was reported previously [26]. Slight shifting of the -C = O band in SD-F4 represents partial molecular level interaction of PLFEE and CMs due to a lower proportion of CMs. While witnessing the -C = O stretching band in the physical mixtures (PM-F4 and PM), it could be observed that there was no substantial change in the stretching frequency in the PMs due to the deficiency of interaction among the PLFEE and the CMs. However, in the case of SD, due to the complete molecular interaction and bonding among PLFEE and CMs, the characteristic peaks of PLFEE were found to be disappeared. A similar result of the disappearance of characteristic peaks of darunavir in the SDs with Kolliphor TPGS was reported previously [71]. The polar groups of PIP (PLFEE), such as carbonyl, piperidine ring N, and methylene deoxy, can form a hydrogen bond with the CMs [26]. Such interactions via H-bonding offer molecular level dispersion of the drug in the 3-dimensional network of CMs, hinder the molecular mobility of the drug, and hinder phase separation/recrystallization, thus anticipated to offer long-term physical stability to the solid dispersion [26, 32]. Additionally, the drug-CMs interaction also provides improved drug solubility and maintenance of a greater degree of supersaturation [32].

HPTLC

The compatibility of the extract (mainly PIP and PLGN) with the formulation excipient was also verified by the HPTLC method. The fingerprints of the developed plate are shown in Fig. 5a–c. Out of various mobile phases, toluene:ethyl acetate (6:4 v/v) offered the best results at retardation factor (Rf) of 0.39 ± 0.003 for PIP, and 0.456 ± 0.0047 for PLGN. The Rf value of PIP and PLGN in the extract (PLFEE) was found to be 0.39 ± 0.0005, and 0.45 ± 0.004, respectively, representing the integrity of PIP and PLGN in the extract. The PM and SD showed the Rf value of PIP (0.39 ± 0.002) and PLGN (0.456 ± 0.0035), which were close to the value obtained for pure components and extract. The fingerprints of the developed plate under 254 nm, 366 nm, and visible light are shown in Fig. 5a–c. The fingerprints (under 245 nm and 366 nm) reflected the presence of chromatographic bands for pure PIP and PLGN in PLFEE, PM, and SD, representing their integrity in the extract, physical mixture, and formulation. Thus, the PLFEE is compatible with the used excipients of the solid dispersion system.

Contact angle

The contact angle was measured to investigate the wettability of PLFEE and SD. The lower the contact angle between the drop of water and the film of solid, the better the wettability [94]. Improved wettability offers enhanced solubility and dissolution. The contact angle (θ) of 0° represents complete wetting, whereas a "θ" of 180° represents no wetting [95]. A contact angle below 65° represents hydrophilicity, and a value higher than 65° represents hydrophobicity [96]. Although the θ can be altered in various solutions, water was frequently used as a wetting solution in such measurements [95, 96]. The mean contact angle (θ_M) against each measurement (step number) for PLFEE and optimized SD is shown in Fig. 5d. The contact angle results of PLFEE (Fig. 5e) and SD (Fig. 5f) revealed that, the SD film have a very low contact angle (θ = 17.04° ± 1.27) and nearly 4.18-fold lesser compared to PLFEE (θ = 71.34° ± 0.913). The SD was found to be hydrophilic, whereas the PLFEE showed hydrophobicity. The lower θ value of SD may be ascribed to the presence of CMs, their porous structure, and their amorphous nature compared to

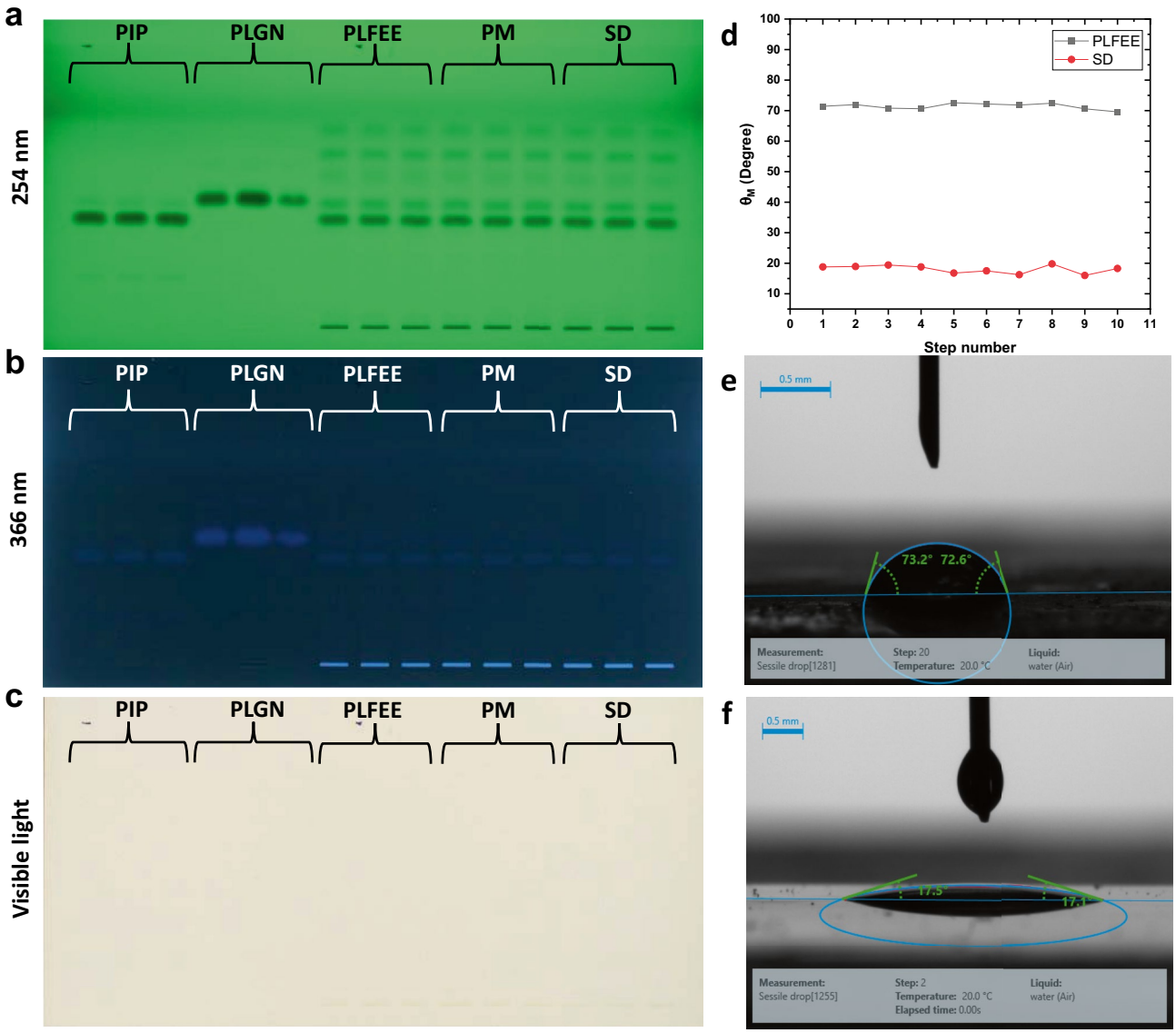

Fig. 5 HPTLC fingerprints of PIP, PLGN, PLFEE, PM, and SD and contact angle measurements; **a** fingerprint under 254 nm, **b** fingerprint under 366 nm, **c** fingerprint under visible light, **d** mean contact angle (θ_M) of 10 individual droplets, **e** contact angle of the water droplet on PLFEE film, and **f** contact angle of the water droplet on SD film

PLFEE. The CMs used in SD are amphiphilic, which reduces the interfacial tension and, ultimately, the θ value.

High-resolution scanning electron microscopy

The HRSEM photomicrographs are shown in Fig. 6a-f. The PLFEE showed irregular surface morphology (Fig. 6a). The Soluplus® showed roughly spherical structures with irregular surface morphology (Fig. 6b). The PM showed agglomerated particles of Soluplus® and PLFEE with irregular surface morphology (Fig. 6c). The Tween® 80 was not distinguished in PM due to its liquid nature which is uniformly coated over the surface of Soluplus® and PLFEE particles. The SD showed irregular particles (Fig. 6d). The individual surface properties of formulation components were not observed in SD due to the complete molecular interaction among PLFEE and CMs owing to the creation of new surface morphology during solvent evaporation. The ethanolic solutions of PLFEE and SD were dried on a glass slide and observed after 14 days for possible crystal growth. The dried PLFEE on the glass slide (Fig. 6e) showed crystalline blocks representing the phenomenon of natural crystal growth. In contrast, the SD dried on the glass slide appeared as a smooth surface without any crystallinity (Fig. 6f), representing the retention of amorphous property and inhibition of nucleation and crystal growth during storage.

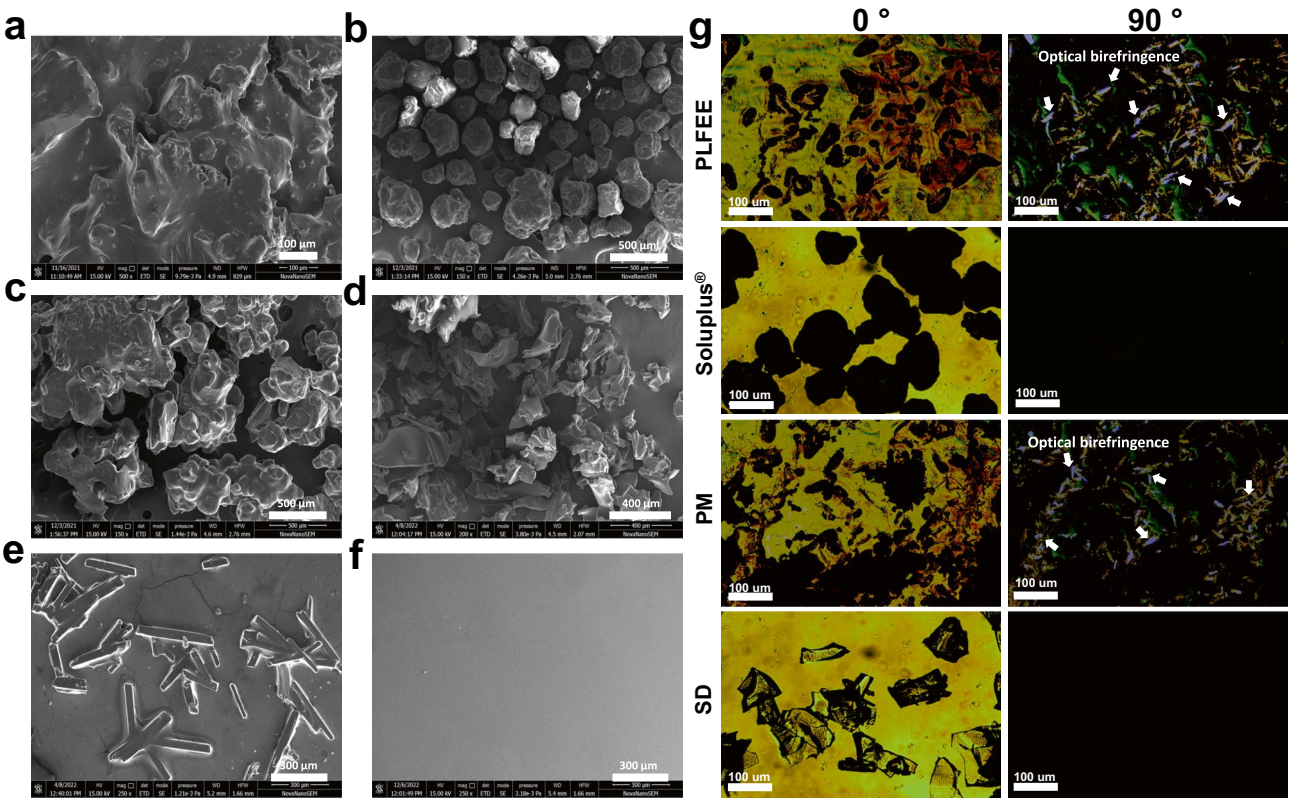

Fig. 6 High-resolution scanning electron microscopy (HRSEM) and polarized light microscopy (PLM) photomicrographs of **a** PLFEE, **b** Soluplus®, **c** PM, **d** SD, **e** PLFEE dried on a slide, **f** SD dried on a slide, and **g** PLM of PLFEE, Soluplus®, PM, and SD at 10 × magnification

Polarized light microscopy

Crystalline materials are optically anisotropic and possess optical birefringence properties. In contrast, amorphous materials (optically isotropic) did not show any birefringence and were observed as a black background. The PLM results of PLFEE, Soluplus®, PM, and SD at 10 × magnification are shown in Fig. 6g. The photomicrographs of the PLFEE demonstrated intense birefringence, reflecting their crystalline nature. The Soluplus® showed no birefringence due to its amorphous nature. The PM showed optical birefringence, representing the retention of crystallinity of PLFEE in PM. In contrast, the SD exhibited no birefringence, suggesting the complete amorphous conversion of crystalline PLFEE in the solid dispersion. The results of PLM are in accordance with the XRD and DSC results.

Moisture content analysis

The moisture content of optimized SD ($n = 3$) measured by the moisture analyzer was found to be 1.124 ± 0.254% which is in accordance with the initial weight loss of 1.324% obtained from the TGA result. A very low amount of moisture in SD may be due to the adsorption of atmospheric moisture during the handling of the sample. The moisture content values of 1.3–5% were reported with SD systems [97, 98]. High moisture content negatively affects the physical stability of SD. The presence of excess moisture can plasticize the system and further reduce the T_g of SD [98].

In vitro dissolution and release kinetics

Poor dissolution is a major rate-limiting step in the oral absorption and bioavailability of poorly aqueous soluble candidates from a solid formulation. Hence, it is of utmost importance to improve the dissolution rate of poorly aqueous soluble drugs to achieve maximum bioavailability and therapeutic efficacy. To assess the impact of CMs, the dissolution pattern of PIP from PLFEE, PM, and SD was studied and compared. The in vitro dissolution profiles of PLFEE, PM, and SD in pH 1.2 are shown in Fig. 7a. The release of PIP from PLFEE, PM, and SD at 2 h was found to be 10.851 ± 3.845%, 29.867 ± 3.5983%, and 87.383 ± 3.546%, respectively. The PLFEE showed low dissolution owing to its poor aqueous solubility, wettability, and high crystallinity. The dissolution of PIP in the case of PM and SD was found to be significantly ($p < 0.05$) enhanced compared to the PLFEE. The SD attained saturation at 6 h. The SD

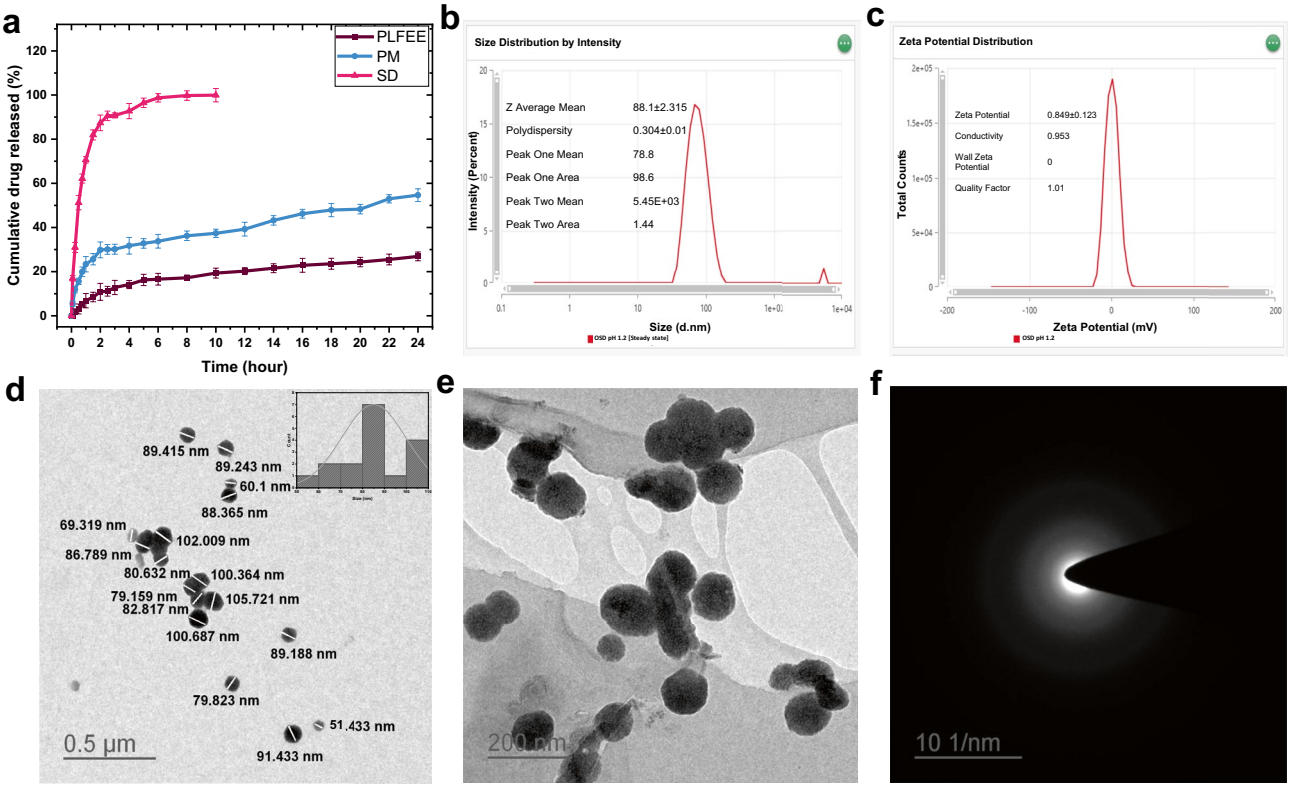

Fig. 7 In vitro dissolution study, hydrodynamic particle size (Z_{avg}), polydispersity index (PDI), zeta potential (ζ), HRTEM photomicrographs, and SAED pattern; **a** dissolution of PLFEE, PM, and SD in pH 1.2, **b** Z_{avg} and PDI of produced micelles, **c** ζ on micelles during dissolution, **d** HRTEM photomicrograph of micelles at 0.5 µM scale with inset image showing size distribution, **e** HRTEM photomicrograph of micelles at 200 nm scale, and **f** SAED pattern of micelles in dissolution media. Each analysis was carried out in triplicate, and the results were represented as mean ± standard deviation

maintains the supersaturation for up to 24 h without any precipitation or decrease in dissolution.

The PM showed improved dissolution compared to the PLFEE and decreased dissolution compared to the SD. The hydrophilic CMs present in the PM possess the surfactant property, which decreases the interfacial tension, causes wetting of the insoluble PIP, solubilizes through micellar solubilization, and ultimately enhances the saturation solubility. However, the PM is a simple physical mixture of PLFEE and CMs, which did not achieve molecular level interaction, retain the drugs in their original size, and possess crystallinity, hence possess comparatively low dissolution than that of SD. In contrast, the SD is a molecular mixture in which size reduction and amorphous modification occur. The enhanced solubility and dissolution of PIP in SD than PM and PLFEE are ascribed to particle size reduction, reduction of diffusion layer thickness due to smaller particle size, increased surface area, increased wetting, decreased interfacial tension, amorphous modification, inhibition of nucleation or crystal growth, and micellar solubilization [26, 46, 65, 68]. The self-assembling behavior of CMs (i.e., Soluplus® and Tween® 80) produces micelles during dissolution and enhances the solubility of PIP through micellar solubilization. The hypothesized diagram of micellar solubilization by SD is shown in Fig. S11. The improved dissolution of SD was further explained through the "spring and parachute" phenomenon. During the dissolution of optimized SD, supersaturation (spring) was achieved, which was found to be maintained for a longer time (parachute), thereby providing a higher amount of dissolved drug for drug absorption. In SDs, drug candidates mostly exist as amorphous forms dispersed within the CMs at the molecular level [65]. During exposure to the dissolution media, the drug candidate dissolves with excipients and creates a supersaturated solution [65]. Owing to the highly energetic amorphous form of the drug in a supersaturated solution, there exists a thermodynamic driving force that permits them to undergo nucleation and crystal growth [65]. However, the CMs in the SDs retain the drug in the metastable amorphous state, inhibit the nucleation and crystal growth and maintain the supersaturation for a prolonged time, and ultimately improve the dissolution [26, 32, 65].

The dissolution data of SD in pH 1.2 was fitted to various kinetic models, and the correlation coefficient (R^2) was

estimated for comparison. Table S11 represents dissolution rate constants (K_0, K_1, K_H, K_{kp}, and K_{HC}), correlation coefficients (R^2), and release exponents (n) of various mathematical kinetic models. The data of SD showed the greatest correlation with the Korsmeyer-Peppas model due to the higher R^2 value (0.916). The goodness of fit of the dissolution behavior of various SDs with the Korsmeyer-Peppas model has been reported by various authors [44, 99, 100]. The mechanism of release was investigated from the Korsmeyer-Peppas model by fitting 60% of the initial dissolution data. The n value of < 0.45, 0.46–0.88, 0.89, and > 0.89 represents fickian diffusion, anomalous diffusion, case II transport, and supercase II transport, respectively [44]. The SD showed anomalous diffusion ($n = 0.6$) in pH 1.2, representing that the mechanism of PIP release was predominantly diffusion-controlled.

Particle size, size distribution, and zeta potential

The average hydrodynamic particle size (Z_{avg}) of SD during dissolution in pH 1.2 was found to be 88.1 ± 2.315 nm (Fig. 7b). The SD during dissolution is suspected of forming micelle in dissolution media, which could enhance the solubility of PLFEE (mainly the PIP) through a micellar solubilization mechanism. The PDI is a measure of homogeneity of particle size distribution which varies from 0 to 1 (perfectly uniform to highly polydisperse) [43]. The formed micelles in pH 1.2 at 37° C were found to be heterogenous, having a PDI of 0.304 ± 0.01 (Fig. 7b). The zeta potential (ζ) is an indication of colloidal stability [50]. The value of zeta potential was found to be 0.894 ± 0.123 mV in pH 1.2 (Fig. 7c). Such low ζ value, nanometric Z_{avg}, and PDI of Soluplus® micelle were reported elsewhere [63].

High-resolution transmission electron microscopy and selected area electron diffraction analysis

The HRTEM results of SD in pH 1.2 at 0.5 µm (Fig. 7d) and 200 nm scale (Fig. 7e) revealed the spherical-shaped nano micellar structure with smooth surface morphology, having a mean micelle size (average size of 17 micelles) of 85.116 ± 14.13 nm. The high standard deviation is due to the heterogeneity of the produced micelles. The size distribution chart revealed that most of the micelles were within the range of 80 to 90 nm (inset Fig. 7d). The SAED results (Fig. 7f) displayed diffused ring pattern, implying the retention of the amorphous form of the SD in pH 1.2.

Stability study

When the SD contained hard gelatin capsules was warped in double-layer aluminum foils and tested under accelerated (40 ± 2 °C and 75 ± 5% RH), intermediate (30 ± 2 °C and 65 ± 5% RH), and long-term (25 ± 2 °C and 60 ± 5% RH) testing conditions, the physical appearance, drug content (97.879 ± 1.57%) and saturation solubility (0.858 ± 0.034) remained unchanged. The optimized SD exposed to 40 ± 2 °C and 75 ± 5% RH maintained its physical integrity when evaluated at 3 months, but after 6 months, it was found to be slightly molten; however, the remaining stability-indicating parameters were found to be unchanged. The slight change in the physical form is due to continuous exposure to high temperature and humidity. Hence, the optimized SD can be best stored at accelerated (40 ± 2 °C and 75 ± 5% RH) conditions for up to 3 months, intermediate (30 ± 2 °C and 65 ± 5% RH) for up to 6 months, and long-term (25 ± 2 °C and 60 ± 5% RH) storage conditions for up to 1 year without alteration of physical form. The XRD (Figs. S12a and S13a) and DSC results (Figs. S12b and S13b) revealed the retention of the amorphous nature of the SD throughout the stability study in all stability conditions. The % weight loss of SD with respect to the temperature observed through TGA analysis remained unaltered, revealing the retention of thermal property (Figs. S12c and S13c). The characteristic vibrational peaks of SD (Figs. S12d and S13d) observed at various time points were found to be retained throughout the stability study without shifting or disappearance of important peaks, signifying the retention of its chemical integrity. The stability of solid dispersions is always troublesome owing to the aging problem. However, the SD showed excellent stability in terms of physical appearance, drug content, saturation solubility, crystallinity, thermal behavior, and chemical composition.

In vitro cytotoxicity

B16F10 melanoma cell line was used as the cancerous cell line, and the human embryonic kidney cell line (HEK 293) was chosen as a non-cancerous (normal) cell line for cytotoxicity comparison. The cytotoxicity results of PLFEE suspension, PLFEE solution, optimized SD, and DTIC against B16F10 and HEK293 after 24 h are presented in Fig. 8a–f. The optimized SD showed improved dose-dependent cytotoxicity against B16F10 cells compared to PLFEE suspension and PLFEE solution (Fig. 8a). The standard anticancer drug, DTIC, also demonstrated dose-dependent cytotoxicity against B16F10 cells (Fig. 8b). The log concentration of PLFEE suspension, PLFEE solution, and optimized SD v/s % cell viability of B16F10 is presented in Fig. 8c. The calculated IC_{50} values of PLFEE suspension, PLFEE solution, optimized SD against B16F10 were found to be 516.51 ± 3.286 ($R^2 = 0.978$), 87.41 ± 2.149 ($R^2 = 0.998$), and 57.25 ± 2.396 µg/mL ($R^2 = 0.985$), respectively. The tested negative control (placebo SD and 0.2% DMSO) did not show any cytotoxicity to the B16F10 cell line (data not shown), indicating the cytotoxicity is only for the standardized

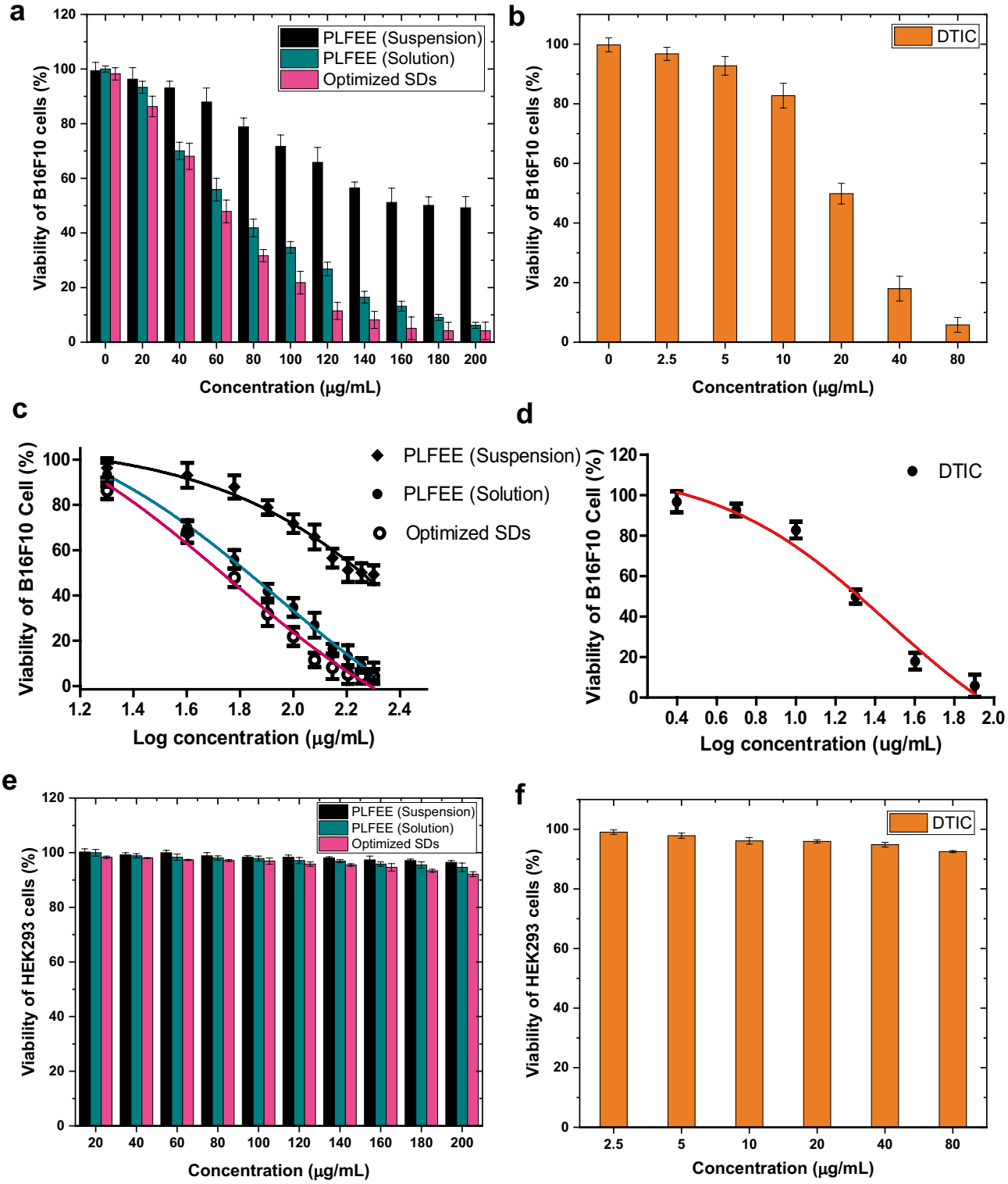

Fig. 8 Cytotoxicity studies; **a** cytotoxicity of PLFEE suspension, PLFEE solution, and optimized SD against B16F10 after 24 h, **b** cytotoxicity of DTIC against B16F10 after 24 h, **c** log (concentration) of PLFEE suspension, PLFEE solution, and optimized SD v/s viability (%) of B16F10 after 24 h, **d** log (concentration) of DTIC v/s viability (%) of B16F10 after 24 h, **e** cytotoxicity of PLFEE suspension, PLFEE solution, and optimized SD against HEK 293 cells after 24 h, and **f** cytotoxicity of DTIC against HEK293 after 24 h. Each data point represents the mean ± SD of three independent experiments

PLFEE and DTIC. The estimated IC_{50} value as per nonlinear regression analysis (Fig. 8d) for DTIC was found to be 29.22 ± 2.172 µg/mL ($R^2 = 0.978$). The tested PLFEE suspension, PLFEE solution, optimized SD, and DTIC showed no cytotoxicity towards the normal HEK 293 cell line (Fig. 8e and f). Such outcomes represent their selective cytotoxicity towards cancer cells without harming the normal cells.

Thus, the important outcomes of the study were that the cytotoxicity of optimized SD against B16F10 melanoma cells was found to be significantly higher ($p < 0.05$) than PLFEE suspension and PLFEE solution (Fig. 8c). The optimized SD improved the cytotoxicity activity of the standardized PLFEE. The higher cytotoxicity of SD might be ascribed to its high cell uptake and partitioning into the cells. During the in vitro assay, the free PLFEE (suspension) diffuses throughout the intracellular environment via the passive diffusion mechanism. Due to the limited solubility and therefore the low concentrations of PLFEE in the surrounding media, low cellular uptake occurred, leading to low cytotoxicity. In contrast, the PLFEE solution (in 0.2% DMSO) showed improved cytotoxicity due to relatively higher concentration in the local media and better diffusion. In the case of optimized SD, it not only improved the solubility in the surrounding media but also improved the partitioning/membrane permeability into the cell due to the micellar formation (as observed previously in Fig. 7d). The micellar property is contributed by the amphiphilic Soluplus® and Tween® 80. The outcome of the cytotoxicity study is in accordance with the reported outcomes of curcumin SD compared to a neat drug, where the authors found improved cytotoxicity of curcumin SD against human glioblastoma (U-87 MG) and breast cancer (MCF-7) cell lines [101]. In the recent work, curcumin SD also showed improved in vitro cytotoxicity against colorectal adenocarcinoma cells (SW480) compared to pure curcumin [102]. In another work, the SD of curcumin also demonstrated improved cytotoxicity against human breast cancer cell line (MDA-MB-23) than that of unformulated curcumin [103].

In vivo oral bioavailability study

The quantitative estimation of PIP in plasma following the oral administration of PLFEE, PM, and SD was done using the validated HPLC method. The detailed validation as per the bioanalytical method is presented in the supplementary file (Section 2.10, Figs. S14 and S15, Tables S12-S17). Mean plasma concentration–time profiles of PIP after oral administration of PLFEE, PM, and optimized SD are presented in Fig. 9a, and the pharmacokinetic (PK) parameters are summarized in Table 5. Compared to the PLFEE, the plasma concentration of PIP was found to be increased following oral administration of SD and PM. One-way ANOVA followed by post hoc Tukey's test was applied to validate significant differences between the mean C_{max} and $AUC_{0\text{-}t}$ obtained for PLFEE, PM, and SD. Differences were considered significant at $p < 0.05$. A significant improvement of C_{max} was obtained for SD (3.278 ± 0.301 µg/mL, $p < 0.01$) and PM (2.013 ± 0.069 µg/mL, $p < 0.05$) compared to PLFEE (1.482 ± 0.235 µg/mL). The C_{max} values of SD and PM are found to be approximately 2.211- and 1.358-fold higher than that of the PLFEE, respectively. The area under the curve from time 0 to 24 h ($AUC_{0\text{-}t}$) of SD (27.001 ± 2.875 µg/mL*h) was found to be significantly higher ($p < 0.01$) than that of PLFEE (14.304 ± 1.365 µg/mL*h). The PM also showed a significant improvement ($p < 0.05$) of $AUC_{0\text{-}t}$ (19.286 ± 2.438 µg/mL*h) compared to PLFEE. The time to reach peak plasma concentration (T_{max}) of PLFEE, PM, and SD was found to be 4 h. The $MRT_{0\text{-}t}$ of PLFEE and PM was found to be 6.770 ± 0.116 h and 6.483 ± 0.126 h, respectively. The $MRT_{0\text{-}t}$ of SD (6.377 ± 0.134 h) was found to be decreased compared to PLFEE, and PM, demonstrating rapid elimination of SD. The relative bioavailability (F_{rel}) of SD and PM were found to be 188.765% and 134.829%, respectively, compared to the PLFEE and are approximately 1.888-fold and 1.348-fold higher than that of neat PLFEE. Dissolution is the rate-limiting step in the oral bioavailability of poorly soluble phytoconstituents, so a small elevation of dissolution rate can enhance oral bioavailability. The findings of the bioavailability study aligned with the results of the in vitro dissolution study, demonstrating that SD provided a noticeable enhancement of dissolution rate compared with crystalline PLFEE and PM. The PM is a simple physical mixture in which the PLFEE still exists in its crystalline form. However, due to the presence of hydrophilic CMs in PM, the dissolution and bioavailability were found to be slightly improved. Moreover, the PK parameters and plasma drug–time profile clearly showed a significant increase in C_{max}, $AUC_{0\text{-}t}$, and F_{rel} of the PIP by the prepared SD. The improved oral bioavailability of SD might be accounted to the following factors: (i) enhanced solubility and dissolution due to amorphous conversion, highly porous structure, increased wetting, and micellar solubilization; (ii) maintenance of supersaturation and prevention of nuclear growth/ precipitation by the CMs (surfactant and polymer); and (iii) improved permeability owing to the amphiphilic behavior of CMs.

Acute oral toxicity study

The study was performed as per OECD 425 guidelines, and the toxicity was reported based on survival or death, decrease in body weight, behavioral alterations, biochemical parameters, hematological parameters, and histopathology. At all doses of standardized PLFEE, rapid movement and disagreeable behavior of animals were observed, which is due to its pungent principle. At the dose of 2000 mg/kg, tremors after 2 h and mortality within 24–48 h were

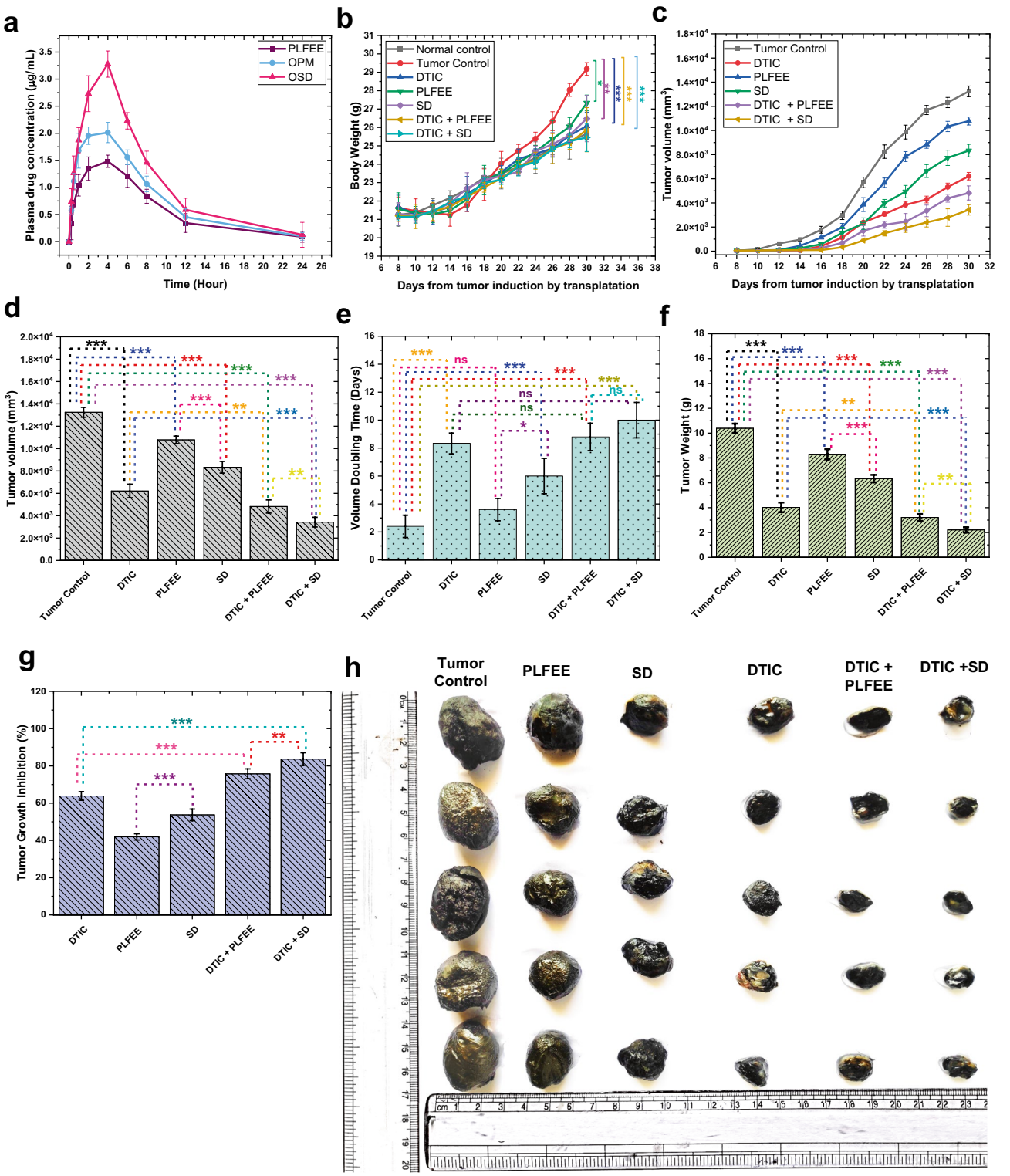

Fig. 9 Oral bioavailability study and tumor regression analysis. **a** Plasma drug concentration–time profile after oral administration of PLFEE, PM, and SD, each equivalent to 62.83 mg/kg of PIP in female SD rats ($n = 5$, Mean ± SD), **b** changes in body weight, **c** tumor volume at an interval of 2 days after developed palpable tumor, **d** tumor volume at the end of dosing (30th day), **e** tumor volume doubling time (VDT) of various group, **f** tumor weight at 30th day, **g** percent tumor growth inhibition (% TGI) of various groups at 30th day, **h** photograph of representative tumors from each group at 30.th day. The asterisk marks (*) represent the level of significance at $p < 0.05$ in all cases. The statistical analysis for the oral bioavailability and tumor regression analysis was performed using one-way ANOVA followed by Tukey's multiple comparison test at $p < 0.05$ using GraphPad Prism 5 (GraphPad Software, Inc., San Diego, CA)

Table 5 Pharmacokinetic (PK) parameters of PIP following single oral administration of PLFEE, PM, and optimized SD ($n = 5$, mean ± SD)

PK parameters	Unit	PLFEE	PM	Optimized SD
C_{max}	µg/mL	1.482 ± 0.235	2.013 ± 0.069*	3.278 ± 0.301**
T_{max}	h	4	4	4
$AUC_{0\text{-}t}$	µg/mL*h	14.304 ± 1.365	19.286 ± 2.438*	27.001 ± 2.875**
$AUC_{0\text{-}\infty}$	µg/mL*h	14.906 ± 2.73	19.912 ± 2.072	27.765 ± 1.946
$t_{1/2}$	h	4.788 ± 0.363	4.506 ± 0.334	4.259 ± 0.517
K_e	1/h	0.144 ± 0.005	0.153 ± 0.004	0.162 ± 0.002
$MRT_{0\text{-}t}$	h	6.770 ± 0.116	6.483 ± 0.126	6.377 ± 0.134
$MRT_{0\text{-}\infty}$	h	7.745 ± 0.29	7.239 ± 0.367	7.031 ± 0.6
Vz/F	(mg/kg)/(µg/mL)	29.116 ± 1.687	20.512 ± 2.816	13.905 ± 0.528
CL/F	(mg/kg)/(µg/mL)/h	4.214 ± 0.097	3.155 ± 0.123	2.262 ± 0.156
F_{rel}	%	-	134.829	188.765

Results are represented as mean ± SD

C_{max} peak plasma concentration, T_{max} time to reach peak plasma concentration, $AUC_{0\text{-}t}$ area under the plasma drug concentration–time curve from time 0 to 24 h, $AUC_{0\text{-}\infty}$ area under the plasma drug concentration–time curve from time 0 to infinity h, $t_{1/2}$ elimination half-life, K_e elimination rate constant, $MRT_{0\text{-}t}$ mean residence time from time 0–24 h, $MRT_{0\text{-}\infty}$ mean residence time from time 0 to infinity h, V_z/F apparent volume of distribution, CL/F apparent systemic clearance following an extravascular (e.v.) administration, and F_{rel} relative bioavailability

*$p < 0.05$ and **$p < 0.01$ when compared with rats administered with PLFEE

observed. In contrast, no tremors or mortality was found at the dose of 550 mg/kg and lower doses when observed over 48 h. The surviving mice (administered with 550 mg/kg) were further observed for 14 days. No death of animals was observed in the case of the 550 mg/kg group after 14 days. A statistically insignificant difference ($p < 0.05$) was noticed between the body weight of the PLFEE (550 mg/kg) treated C57BL/6 group (21.786 ± 1.423 g) and the vehicle control C57BL/6 group (21.273 ± 1.123 g) on the 15th day. The initial body weight was found to be slightly increased in both cases, which is due to the normal physiological growth of the body. The biochemical (Table S18) and hematological parameters (Table S19) of the PLFEE (550 mg/kg) treated C57BL/6 group and vehicle control C57BL/6 group, studied after 14 days, reflected a non-significant difference ($p < 0.05$). Further, no signs of toxicity and histological alterations of the vital organs were observed between the PLFEE (550 mg/kg) treated C57BL/6 group and the vehicle control C57BL/6 group (Fig. S16). A detailed histological description was provided in the supplementary file (Section 2.12). The overall results revealed no sign of toxicity in the C57BL/6 animals after the administration of 550 mg/kg of standardized PLFEE. The calculated LD_{50} value (provided by the AOT425statpgm software) of PLFEE against C57BL/6 mice was 1098 mg/kg at a 95% level of confidence.

In vivo anticancer activity against melanoma

Based upon the reported in vitro and in vivo anticancer activities of various alkaloids present in the *P. longum* fruits and whole extract against melanoma [19–23, 25], the in vivo anticancer activity of the optimized ternary SDs was evaluated and compared with standardized PLFEE. Most of the phytoconstituents of the PLFEE are hydrophobic, which suffers from poor dissolution, bioavailability, and low therapeutic activity. So, to realize the real therapeutic potential of the PLFEE, improvement in the solubility and bioavailability is essential. After investigation and confirmation of improved solubility, in vitro dissolution profile, in vivo oral bioavailability, and in vitro cytotoxicity against melanoma (B16F10) cell line of PLFEE, the in vivo anticancer activity of optimized SDs were evaluated and compared with standardized PLFEE.

The in vivo syngeneic experimental tumor model was established by subcutaneous implantation of highly metastatic B16F10 murine cancer cells to the C57BL/6 mice. This model allows the interaction of melanoma cells with T-cells and B-cells, thus possessing an advantage over the xenografts model in which immunosuppressed mice were used [104]. The treatments were started 8 days after the tumor induction and continued up to the 30th day. The body weight and tumor volume were evaluated throughout the treatment period. The tumor regression study of 30 days was conducted based on the available literature. Thirty days of tumor regression studies have been reported for *Cinnamomum cassia* extract on in vivo melanoma growth in C57BL/6 mice [105, 106]. Even 15 days of studies were also reported previously, where authors had studied the effect of andrographolide on in vivo tumor growth in C57BL/6 mice [107]. In other studies, a minimum of 22 days (15 days after palpable tumor, i.e., ~ 7 days) [108], 20 days [109], and 21 days [53] were also studied for tumor regression analysis. In most

cases, tumor regression studies were performed for up to 30 days. Further, we have also noticed slight rupture and oozing of fluid at the surface of solid tumor after 35 days in our pilot studies. Considering the above factors, the tumor regression study was conducted for 30 days.

The dose of the standardized PLFEE (200 mg/kg b.wt) was selected based on our pilot studies on tumor regression studies, where we have obtained statistically significant tumor regression outcomes. The dose of DTIC (5 mg/kg i.p. every 2 days) was selected based on the reported literature, where authors have reported the combination therapy of dacarbazine and statins to improve the survival rate of C57BL/6 J mice with metastatic melanoma [53].

The changes in the body weight during the study were recorded to monitor the in vivo tumor growth. The normal control group showed a gradual increase in body weight up to the 30th day. The tumor control group showed an initial loss of body weight followed by faster weight gain than the treated groups and normal control group due to uncontrolled tumor growth (Fig. 9b). In contrast, the body weight of all treated groups was found to be significantly lower ($p < 0.05$) than that of the "tumor control group" due to the treatment effects.

The results of tumor volume of C57BL/6 mice of various groups (untreated and treated) during the treatment period and at the end of the study are shown in Fig. 9c and d, respectively. The "tumor control group" represented a higher overall TV than the treated groups (Fig. 9c). The calculated TV was in the order of "tumor control group" > "PLFEE group" > "SD group" > "DTIC grou p" > "DTIC + PLFEE" > "DTIC + SD" group (Fig. 9d). A significant decrease ($p < 0.05$) in the tumor volume was noticed in the treated group compared to the tumor control group (vehicle-treated) on the 30th day of tumor induction. The standardized PLFEE alone significantly reduced ($p < 0.05$) the TV compared to the "tumor control group." Further, the optimized SD significantly decreased ($p < 0.05$) the TV compared to the "tumor control group" and standardized "PLFEE group." The marked reduction of TV in the case of optimized SD was due to the improved absorption and greater bioavailability of the hydrophobic phytoconstituents compared to the neat PLFEE. In the case of the "standard drug group," the DTIC exhibited a significant reduction ($p < 0.05$) of the tumor volume compared to the "tumor control group." When the standardized PLFEE was used as an adjuvant to the DTIC, a significant reduction ($p < 0.05$) of the TV was noticed compared to the DTIC alone and "tumor control group" on the 30th day. Further, in the case of the "DTIC + SD"–treated group, a remarked decrease and significant reduction ($p < 0.05$) of TV was found compared to the "DTIC + PLFEE" group, ascribed to the improved bioavailability of phytoconstituents when administered in the form of SD.

The VDT (in days) of various treatment groups was found to be increased compared to the "tumor control" group due to the treatment effects (Fig. 9e). The "PLFEE group" showed a non-significant difference in the VDT compared to the "tumor control" group. The VDT value in the case of the optimized "SD group" was found to be significantly higher ($p < 0.05$) than that of the PLFEE-treated and tumor control group. The "DTIC group" demonstrated a significant improvement in the VDT ($p < 0.05$) compared to the "tumor control." A significant prolongation of the VDT ($p < 0.05$) was noticed in the case of "DTIC + PLFEE group" compared to the "tumor control group." However, at 95% level of significance, a non-significant difference in the VDT was noticed between the "DTIC + PLFEE" group and the DTIC group. The "DTIC + SD group" demonstrated a significant lengthening of the VDT ($p < 0.05$) compared to the "tumor control group" but a non-significant difference in the VDT was observed between "DTIC + SD group" and "DTIC + PLFEE" group. At a 95% level of significance, all the treatment groups showed prolongation of VDT compared to "tumor control" group. However, some non-significant differences in the VDT among various treatment groups are due to the uncontrolled rapid cell proliferation at the beginning of the tumor progression. During the study, it was observed that most of the tumors attained double of their initial volume within 8 ± 1 days. So, among some of the treatments, a statistical significance difference was not established.

The results of isolated tumor weight at the end of the study are represented in Fig. 9f. The tumor control group showed the highest tumor weight. In contrast, all the treatment groups showed a significantly lower ($p < 0.05$) tumor weight. The tumor weight in the case of the standardized "PLFEE group" was found to be significantly reduced ($p < 0.05$) compared to the "tumor control group." Further, the optimized SD significantly decreased ($p < 0.05$) the tumor weight compared to the standardized "PLFEE group" and "tumor control group" due to its improved absorption and greater bioavailability compared to the neat PLFEE. In the case of the DTIC-treated group, a significant loss ($p < 0.05$) of the tumor weight was noticed compared to the "tumor control group." The "DTIC + PLFEE group" further decreased the tumor weight compared to the DTIC alone and "tumor control group" on the 30th day. Further, in the case of the "DTIC + SD"–treated group, a significant loss of tumor weight ($p < 0.05$) was observed compared to the "DTIC + PLFEE" group and "tumor control group." Hence, the optimized SD can be used as an effective adjuvant therapy with DTIC than standardized PLFEE.

The % TGI was found to be significantly increased ($p < 0.05$) in the case of treated groups compared to the tumor control group (Fig. 9g). Except for PLFEE (% TGI = 41.89774 ± 1.684%), all the treatment groups showed a TGI of more than 50%. A % TGI of > 50% was considered to

be meaningful [14]. The SD-treated group showed a significant improvement ($p < 0.05$) of % TGI compared to the PLFEE-treated group. The "DTIC + PLFEE" group demonstrated a significant improvement of % TGI compared to the standard drug (DTIC) alone, representing the efficiency of adjuvant therapy. Further, the "DTIC + SD" group showed a significant enhancement of % TGI compared to the "DTIC + PLFEE" group, representing the higher efficacy of adjuvant therapy when the PLFEE is administered as SD form.

The photograph of representative tumors from each group at 30th day is shown in Fig. 9h. The extracted tumors showed treatment-dependent anticancer outcomes (tumor volume) as stated above.

The histopathological results of tumor tissue of various groups supplementary file (Section 2.13, Fig. S17) reflected the higher antitumor activity of optimized SD compared to the PLFEE. Further, SD as an adjuvant medication also enhanced the anticancer activity of DTIC for melanoma therapy.

Similar tumor regression outcomes were reported for a hydro-methanolic extract from leaf, stem bark, and flower of *Bauhinia variegate* in B16F10 cell–bearing C57BL/6 mice. The author reported a statistically significant difference ($p < 0.05$) between the untreated control group and treated groups at a dose of 500 and 750 mg/kg b.wt. every alternate day for up to 40 days [14]. In another work, aqueous bark extract of *Cinnamomum cassia* was investigated against in vivo murine melanoma model using C57BL/6 mice. A significant decrease in the tumor volume and weight was reported by the authors when orally administered at a dose of 10 mg/dose for up to 30 days [105, 106]. The tumor volume and weight of the control group of these studies are as per our observed TV values for tumor control group. However, the treatment effects are different due to the inherent anticancer properties of the plant extracts.

Numerous plant extracts and phytoconstituents have been reported for melanoma therapy for their ability to suppress melanoma through the regulation of oxidative status, modulation of immunity, correction of disordered replication and induction of apoptosis, and prevention of invasion, angiogenesis, and metastasis [3, 15]. Cancer cells utilize multiple mechanisms for their development, progression, invasion, angiogenesis, and metastasis. Hence, it is rational to use plant extract or fraction (containing numerous phytoconstituents) that may act synergistically in a multi-targeting manner rather than a single constituent or drug molecule.

The extract of *P. longum* fruit and its constituents have shown their anticancer activity against melanoma. The PIP was reported to inhibit transcription factors, such as CREB, AP-1, NF-kβ, and proinflammatory cytokines expression (IL-6, IL-1β, GM-CSF, and TNF-α) in B16F10 (melanoma) cells [19]. It was also reported to cause G1 phase arrest and apoptosis induction in B16F0 and SK MEL 28 melanoma cells through activation of checkpoint kinase-1 (Chk1). Mainly, the generation of ROS by PIP in melanoma cells is involved in inducing G1 cell cycle arrest through the activation of Chk1 [20]. Further, the PIP was also studied for inhibition of lung metastasis in the B16F10 cell–induced tumor model in C57BL/6 mice [21]. The compound piperlongumine was reported to produce cytotoxicity against A375, A875, and B16F10 and induce apoptosis via reactive oxygen species–mediated disruption of mitochondria [22]. The PLGN was also reported to suppress melanogenesis via the downregulation of tyrosinase expression in the melanin synthesis pathway [23], and inhibition of melanogenesis seems a rational adjuvant approach for the treatment of metastatic melanoma [24]. The 70% ethanolic extract of *P. longum* fruit also demonstrated in vitro and in vivo antiangiogenic activities via inhibition of VEGF, tumor-directed capillary formation, and inhibition of proinflammatory cytokines [25].

The investigated standardized PLFEE demonstrated in vitro cytotoxicity against B16F10 cells without affecting normal HEK 293 cell line (Fig. 8a, c, e). The standardized PLFEE alone showed significant ($p < 0.05$) in vivo anticancer activity with tumor regression outcomes compared to the vehicle-treated tumor control group on the 30th day of tumor induction. The therapeutic activity of standardized PLFEE (dose of 200 mg/kg) is attributed to the aforementioned reported anticancer mechanisms [19–23, 25]. The administered oral dose of 200 mg/kg of PLFEE was fixed as per the pilot studies. The optimized SD showed improved in vivo tumor regression results compared to unformulated standardized PLFEE. The significantly higher ($p < 0.05$) in vivo anticancer activity of SD is ascribed to its improved dissolution, oral absorption, and bioavailability. Further, the micelles generated from SD may be passively targeted to the tumor microenvironment by the enhanced permeation and retention (EPR) effect, resulting in improved anticancer activity.

The standard anticancer drug, DTIC, exhibited a significant ($p < 0.05$) tumor regression outcome compared to the tumor control group, standardized PLFEE, and SD group. DTIC is the only Food and Drug Administration (FDA)–approved first-line chemotherapeutic drug for melanoma therapy, which is a strong alkylating agent. Its anticancer activity is ascribed to the destruction of cancer cells by adding an alkyl group to their DNA [110]. When the standardized PLFEE was used as an adjuvant to the DTIC, significant ($p < 0.05$) tumor regression outcomes were observed compared to the DTIC alone and tumor control group on the 30th day. The synergistic anticancer activity of DTIC with the PLFEE is ascribed to the additive inherent anticancer activity of the contained phytoconstituents in PLFEE and the alkylating property of DTIC. The major bioactive phytoconstituent, PIP, was reported to act as a herbal bioenhancer that increases the bioavailability of drugs by promoting (i) rapid absorption of drugs or (ii) by inhibiting the enzymatic drug metabolism. It is also a potent inhibitor of the P-glycoprotein (P-gp) efflux pump and principal metabolizing enzyme CYP3A4 [111]. ATP-binding cassette (ABC)

transporters (mainly the P-gp) are expressed at membranes of cancer cells that induce multidrug resistance. Relatively minor improvements in drug resistance are sufficient to render treatment ineffective in cancer cells. The use of P-gp inhibitors with chemotherapeutic drugs has been previously verified to overcome multidrug resistance [111, 112]. Many of the phytochemicals, including PIP, quercetin, naringin, genistein, sinomenine, curcumin, allicin, capsaicin, and glycyrrhizin, have been reported to act as herbal bioenhancer [111, 113]. The DTIC was reported to be effluxed by the P-gp pump [114]; thus, its inhibition by the PIP contained in the standardized PLFEE might be responsible for synergistic anticancer activity. DTIC is a pro drug, which catalytic activation by liver cytochromes P450 enzymes (mainly by CYP1A1, CYP1A2, and CYP2E1) is required for anticancer activity [115]. However, PIP is reported to possess an inhibitory effect on the principal metabolizing enzyme CYP3A4 [111]. Thus, the metabolic inhibition by the PIP may not contribute to improved anticancer activity. Hence, the improved anticancer activity of DTIC when administered with PLFEE might be attributed to the inherent anticancer activity of the standardized PLFEE and the P-gp efflux inhibition. Further, in the case of the "DTIC + SD"–treated group, a significant ($p < 0.05$) anticancer activity was found compared to the "DTIC + PLFEE" group, ascribed to the improved bioavailability of phytoconstituents when administered in the form of SD.

Summary and conclusion

The development and identification of new anticancer agents are time-consuming and costly. The side effects of currently used chemotherapeutics are a major issue for cancer treatment despite their strong anticancer activity. Thus, the search for an alternative therapy with limited side effects and toxicity is an important area of research. Plant-based substances (crude drug, extract, fraction, or isolated phytoconstituents) have shown their excellency in the therapy of numerous tumors in multiple molecular mechanisms. Further, plant-based therapeutics can be used as an alternative as well as supportive therapy to the current chemotherapeutics. Among various skin cancers, melanoma is one of the most aggressive and deadly forms. Numerous plant extracts as well as isolated phytoconstituents have been well exploited for melanoma therapy [3, 15]. Melanoma cells utilize various mechanisms (disordered replication and evasion of apoptosis, angiogenesis, tissue invasion, metastasis, modulation of the immune system, and oxidative reactions) for their rapid growth and development [3]. Hence, it is logical to use plant extract that will act synergistically in a multi-targeting manner rather than a single constituent or drug molecule. Various plants have been reported to act against melanoma through the inhibition of the aforementioned mechanisms [3].

The in vivo anticancer activity of standardized PLFEE was studied and compared with that of the optimized SD formulation. The marker-based standardization of the PLFEE with respect to PIP and PLGN was carried out to maintain batch-to-batch consistency and to provide dose uniformity. Due to the limited aqueous solubility of the phytoconstituents in the PLFEE, the 4th generation solid dispersion was developed with the use of Soluplus® and Tween® 80. The solvent evaporation by rotatory vacuum evaporation was utilized for the development of solid dispersion and optimized by the QbD approach. The RSM was used to analyze the influence of various factors on saturation solubility as a response. The numerical and graphical optimization was carried out and the outcomes of the software-suggested formula were validated by formulating and analyzing the response. The SD showed amorphous properties with good drug content, content uniformity, wettability, and low moisture content. The ATR-FTIR and HPTLC results revealed the absence of any incompatibility among the extract and the excipients of the SD. The HRSEM revealed the homogeneous irregular morphology of SD. The in vitro dissolution study revealed the improved dissolution profile of SD compared to the physical mixture (PM) and PLFEE. The DLS and HRTEM results of the dissolution sample revealed the formation of micelle during the dissolution, resulting in micellar solubilization and improved dissolution. The stability study revealed the prolonged maintenance of physicochemical and pharmaceutical properties without any alterations. The in vivo oral bioavailability result of SD reflected a significant ($p < 0.05$) improvement of bioavailability (C_{max} and AUC) compared to neat extract and PM. The acute oral toxicity study (OECD 425) via hematological, biochemical, and histopathological observations revealed the non-toxic nature of the standardized PLFEE at the chosen dose. The effect of SD was studied in the syngeneic transplantation model in melanoma (B16F10)–bearing C57BL/6 mice. The results of the tumor regression study revealed improved therapeutic activity of SD compared to neat PLFEE. Further, the SD also improved the anticancer activity of DTIC as an adjuvant therapy. The overall results revealed the potential of developed PLFEE contained SD for melanoma cancer therapy either alone or as an adjuvant therapy with DTIC.

Supplementary Information The online version contains supplementary material available at https://doi.org/10.1007/s13346-023-01375-y.

Acknowledgements The authors are very much thankful to the infrastructural and instrumental facilities provided by the Central Instrument Facility, IIT (BHU); Department of Pharmaceutical Engineering & Technology, IIT (BHU); Department of Physics, IIT (BHU); and Centre for Genetics Disorders, BHU Varanasi, India. The sophisticated analytical instrument facility (SAIF), Indian Institute of Technology (IIT), Mumbai, India, and Rajiv Gandhi Centre for Biotechnology, Thiruvananthapuram, Kerala, India, were also highly acknowledged for GCHS analysis and DNA-based molecular characterization, respectively.

Author contribution Debadatta Mohapatra performed most of the experimental works, collected, processed, analyzed, validated, interpreted data, and wrote the original manuscript. Dulla Naveen Kumar, Singh Shreya, and Vivek Pandey participated in the experiment, reviewed, edited, and scientifically revised the manuscript. Alakh N Sahu, Ashish Kumar Agrawal, and Pawan K. Dubey contributed to conceptualization, project administration, supervision, experiment designing, evaluating, drawing conclusions from data, providing expert assistance, reviewing, and editing the manuscript.

Funding The financial support for this research was provided as a scholarship to Debadatta Mohapatra by the Ministry of Human Resource Development (MHRD), Government of India. The authors declare that this research did not receive any specific grant from funding agencies in the public, commercial, or not-for-profit sectors.

Availability of data and materials All the data are encompassed in this manuscript. The scientific data in terms of graphs and figures were generated using MS office package, a 21-day free trial version of Origin Pro 2021 (Microcal Software, Inc., Northampton, USA), GraphPad Prism 5.0 (GraphPad Software Inc., San Diego, CA, USA), and ImageJ software (National Institutes of Health, Bethesda, MD).

Declarations

Ethical approval The experiments on animals were carried out following an approved protocol from Institutional Animal Ethics Committee (IAEC Approval Number: IIT(BHU)/IAEC/2022/001 and IIT(BHU)/IAEC/2023/056).

Consent to participate Not applicable.

Consent for publicatioon Not applicable.

Conflict of interest The authors declare no competing interests.

References

1. National Institutes of Health (NIH)-2023, National Cancer Institute (NCI), Cancer stat facts: melanoma of the skin; https://seer.cancer.gov/statfacts/html/melan.html.
2. International Agency for Research on Cancer (IARC)-2023, World Health Organization (WHO), Cancer Today, Estimated number of new cases of melanoma of skin in 2020 among both sexs at all ages; https://gco.iarc.fr/today/online-analysis-pie?v=2020&mode=population&mode_population=continents&population=900&populations=900&key=total&sex=0&cancer=16&type=0&statistic=5&prevalence=0&population_group=0&ages_group%5B%5D=0&ages_group%5B%5D=17&nb_items=7&group_cancer=0&include_nmsc=1&include_nmsc_other=1&half_pie=0&donut=0
3. Albuquerque KRS, Pacheco NM, del Rosario Loyo Casao T, de Melo FCSA, Novaes RD, Gonçalves RV. Applicability of plant extracts in preclinical studies of melanoma: a systematic review. Mediators Inflamm.
4. Gilchrest BA, Eller MS, Geller AC, Yaar M. The pathogenesis of melanoma induced by ultraviolet radiation. N Engl J Med. 1999;340(17):1341–8.
5. Postow MA, Hamid O, Carvajal RD. Mucosal melanoma: pathogenesis, clinical behavior, and management. Curr Oncol Rep. 2012;14(5):441–8.
6. Rastrelli M, Tropea S, Rossi CR, Alaibac M. Melanoma: epidemiology, risk factors, pathogenesis, diagnosis and classification. In Vivo. 2014;28(6):1005–11.
7. Li J, Zhang Y, Tao J. Targeted nanoparticles for drug delivery to melanoma: from bench to bedside. In: Nanoscience in dermatology. Elsevier. 2016;203–215.
8. Russo AE, Torrisi E, Bevelacqua Y, Perrotta R, Libra M, McCubrey JA, Spandidos DA, Stivala F, Malaponte G. Melanoma: molecular pathogenesis and emerging target therapies. Int J Oncol. 2009;34(6):1481–9.
9. Li J, Wang Y, Liang R, An X, Wang K, Shen G, Tu Y, Zhu J, Tao J. Recent advances in targeted nanoparticles drug delivery to melanoma. Nanomedicine. 2015;11(3):769–94.
10. Kratz F, Senter P, Steinhagen H. Drug delivery in oncology: from basic research to cancer therapy. John Wiley & Sons; 2013.
11. Newman DJ, Cragg GMJJONP. Natural products as sources of new drugs over the nearly four decades from 01/1981 to 09/2019. 2020;83(3):770–803.
12. Dehelean CA, Marcovici I, Soica C, Mioc M, Coricovac D, Iurciuc S, Cretu OM, Pinzaru I. Plant-derived anticancer compounds as new perspectives in drug discovery and alternative therapy. Molecules. 2021;26(4):1109.
13. Garcia-Oliveira P, Otero P, Pereira AG, Chamorro F, Carpena M, Echave J, Fraga-Corral M, Simal-Gandara J, Prieto MA. Status and challenges of plant-anticancer compounds in cancer treatment. Pharmaceuticals. 2021;14(2):157.
14. Pandey S. In vivo antitumor potential of extracts from different parts of Bauhinia variegata linn. Against b16f10 melanoma tumour model in c57bl/6 mice. Appl Can Res. 2017;37(1):1–14
15. Kinjo J, Nakano D, Fujioka T, Okabe H. Screening of promising chemotherapeutic candidates from plants extracts. J Nat Med. 2016;70(3):335–60.
16. Kumar S, Kamboj J, Sharma S. Overview for various aspects of the health benefits of Piper longum linn. fruit. J Acupunct Meridian Stud. 2011;4(2):134–40
17. Tiwari A, Mahadik KR, Gabhe SYJMIDD. Piperine: a comprehensive review of methods of isolation, purification, and biological properties. 2020;7:100027.
18. National Institute of Health (NIH), U.S. National Library of Medicine; https://clinicaltrials.gov/ct2/results?cond=Piperine%2C+cancer&term=&cntry=&state=&city=&dist=.
19. Pradeep C, Kuttan G. Piperine is a potent inhibitor of nuclear factor-κB (NF-κB), c-Fos, CREB, ATF-2 and proinflammatory cytokine gene expression in B16F–10 melanoma cells. Int Immunopharmacol. 2004;4(14):1795–803.
20. Fofaria NM, Kim S-H, Srivastava SK. Piperine causes G1 phase cell cycle arrest and apoptosis in melanoma cells through checkpoint kinase-1 activation. PLoS ONE. 2014;9(5): e94298.
21. Pradeep C, Kuttan G. Effect of piperine on the inhibition of lung metastasis induced B16F–10 melanoma cells in mice. Clin Exp Metastasis. 2002;19(8):703–8.
22. Song X, Gao T, Lei Q, Zhang L, Yao Y, Xiong J. Piperlongumine induces apoptosis in human melanoma cells via reactive oxygen species mediated mitochondria disruption. Nutr Cancer. 2018;70(3):502–11.
23. Kim KS, Kim JA, Eom SY, Lee SH, Min KR, Kim Y. Inhibitory effect of piperlonguminine on melanin production in melanoma B16 cell line by downregulation of tyrosinase expression. Pigment Cell Res. 2006;19(1):90–8.
24. Brożyna AA, Jóźwicki W, Carlson JA, Slominski AT. Melanogenesis affects overall and disease-free survival in patients with stage III and IV melanoma. Hum Pathol. 2013;44(10):2071–4.

25. Sunila E, Kuttan G. Piper longum inhibits VEGF and pro-inflammatory cytokines and tumor-induced angiogenesis in C57BL/6 mice. Int Immunopharmacol. 2006;6(5):733–41.
26. Thenmozhi K, Yoo YJ. Enhanced solubility of piperine using hydrophilic carrier-based potent solid dispersion systems. Drug Dev Ind Pharm. 2017;43(9):1501–9.
27. Smilkov K, Ackova DG, Cvetkovski A, Ruskovska T, Vidovic B, Atalay M. Piperine: old spice and new nutraceutical? Curr Pharm Des. 2019;25(15):1729–39.
28. Aodah A, Pavlik A, Karlage K, Myrdal PB. Preformulation studies on piperlongumine PloS one. 2016;11(3): e0151707.
29. Zhang X, Xing H, Zhao Y, Ma Z. Pharmaceutical dispersion techniques for dissolution and bioavailability enhancement of poorly water-soluble drugs. Pharmaceutics. 2018;10(3):74.
30. Khadka P, Ro J, Kim H, Kim I, Kim JT, Kim H, Cho JM, Yun G, Lee J. Pharmaceutical particle technologies: an approach to improve drug solubility, dissolution and bioavailability. Asian J Pharm Sci. 2014;9(6):304–16.
31. Williams HD, Trevaskis NL, Charman SA, Shanker RM, Charman WN, Pouton CW, Porter CJ. Strategies to address low drug solubility in discovery and development. Pharmacol Rev. 2013;65(1):315–499.
32. Mohapatra D, Agrawal AK, Sahu AN. Exploring the potential of solid dispersion for improving solubility, dissolution & bioavailability of herbal extracts, enriched fractions, and bioactives. J Microencapsul. 2021;38(7–8):594–612.
33. Gala UH, Miller DA. Williams III RO (2020) Harnessing the therapeutic potential of anticancer drugs through amorphous solid dispersions. Biochim Biophys Acta Rev Cancer. 1873;1: 188319.
34. Chiou WL, Riegelman S. Pharmaceutical applications of solid dispersion systems. J Pharm Sci. 1971;60(9):1281–302.
35. Huang Y, Dai W-G. Fundamental aspects of solid dispersion technology for poorly soluble drugs. Acta Pharm Sin B. 2014;4(1):18–25.
36. Jermain SV, Brough C, Williams RO III. Amorphous solid dispersions and nanocrystal technologies for poorly water-soluble drug delivery–An update. Int J Pharm. 2018;535(1–2):379–92.
37. Allawadi D, Singh N, Singh S, Arora S. Solid dispersions: a review on drug delivery system and solubility enhancement. ChemInform. 2014;45(18):no-no.
38. Connors K, Higuchi T. Phase solubility techniques. Adv Anal Chem Instrum. 1965;4(2).
39. Ha E-S, Baek I-h, Cho W, Hwang S-J, Kim M-S. Preparation and evaluation of solid dispersion of atorvastatin calcium with Soluplus® by spray drying technique. Chem Pharm Bull. 2014;62(6):545–51.
40. Shaker MA. Dissolution and bioavailability enhancement of Atorvastatin: Gelucire semi-solid binary system. J Drug Deliv Sci Technol. 2018;43:178–84.
41. Kyaw Oo M, Mandal UK, Chatterjee B. Polymeric behavior evaluation of PVP K30-poloxamer binary carrier for solid dispersed nisoldipine by experimental design. Pharm Dev Technol. 2017;22(1):2–12.
42. Saoji SD, Dave VS, Dhore PW, Bobde YS, Mack C, Gupta D, Raut NA. The role of phospholipid as a solubility-and permeability-enhancing excipient for the improved delivery of the bioactive phytoconstituents of Bacopa monnieri. Eur J Pharm Sci. 2017;108:23–35.
43. Rahman SNR, Pawde DM, Katari O, Hmingthansanga V, Shunmugaperumal T. Systematic optimization, in vitro drug release, and preliminary nonclinical toxicity assessment of nonphospholipid-based topical ophthalmic emulsions containing 0.05 or 0.1% w/w cyclosporin A for dry-eye syndrome management. AAPS Pharm Sci Tech. 21 2020;(2):36.
44. Sharma N, Singh S. Central composite designed ezetimibe solid dispersion for dissolution enhancement: synthesis and in vitro evaluation. Ther Deliv. 2019;10(10):643–58.
45. Khar RK. Lachman/liebermans: the theory and practice of industrial pharmacy. Cbs Publishers & Distribu. 2013.
46. Shamma RN, Basha M. Soluplus®: a novel polymeric solubilizer for optimization of carvedilol solid dispersions: formulation design and effect of method of preparation. Powder Technol. 2013;237:406–14.
47. Pramod K, Suneesh CV, Shanavas S, Ansari SH, Ali J. Unveiling the compatibility of eugenol with formulation excipients by systematic drug-excipient compatibility studies. J Anal Sci Technol. 2015;6(1):1–14.
48. Gouda R, Baishya H, Qing Z. Application of mathematical models in drug release kinetics of carbidopa and levodopa ER tablets. J Dev Drugs. 2017;6(02):1–8.
49. Kumar DN, Chaudhuri A, Dehari D, Shekher A, Gupta SC, Majumdar S, Krishnamurthy S, Singh S, Kumar D, Agrawal AKJL. Combination therapy comprising paclitaxel and 5-fluorouracil by using folic acid functionalized bovine milk exosomes improves the therapeutic efficacy against breast cancer. 2022;12(8):1143.
50. Mohapatra D, Alam MB, Pandey V, Pratap R, Dubey PK, Parmar AS, Sahu AN. Carbon dots from an immunomodulatory plant for cancer cell imaging, free radical scavenging and metal sensing applications. Nanomedicine. 2021;16(23):2039–59.
51. Zhang Y, Huo M, Zhou J, Xie S. PKSolver: an add-in program for pharmacokinetic and pharmacodynamic data analysis in Microsoft Excel. Comput Methods Programs Biomed. 2010;99(3):306–14.
52. OECD guidelines for the testing of chemicals : acute oral toxicity – up-and-down-procedure (UDP); https://www.oecd.org/env/test-no-425-acute-oral-toxicity-up-and-down-procedure-9789264071049-en.htm.
53. Tsubaki M, Takeda T, Obata N, Kawashima K, Tabata M, Imano M, Satou T, Nishida S. Combination therapy with dacarbazine and statins improved the survival rate in mice with metastatic melanoma. J Cell Physiol. 2019;234(10):17975–89.
54. Gorgani L, Mohammadi M, Najafpour GD, Nikzad M. Piperine—the bioactive compound of black pepper: from isolation to medicinal formulations. Compr Rev Food Sci Food Saf. 2017;16(1):124–40.
55. United States Pharmacopeia (USP) 30, 〈467〉, Residual solvents, VERSION-8/TEMPLATE/V8_USPNF/V8_USPNF.3F; https://www.uspnf.com/sites/default/files/usp_pdf/EN/USPNF/generalChapter467Current.pdf.
56. Impurities: guideline for residual solvents Q3C(R8), Step 4 version, 22 April 2021. International Council for Harmonisation of Technical Requirements for Pharmaceuticals for Human use, ICH Harmonised Guideline; https://database.ich.org/sites/default/files/ICH_Q3C-R8_Guideline_Step4_2021_0422_1.pdf.
57. Sahu A N and Mohapatra D, Herbal drug formulation and standardization. 1 edn. (21 June 2021), ISBN-10: ‎9390658365,ISBN-13: ‎978-9390658367, Ane Books Pvt Ltd., Darya Ganj, New Delhi - 110002.
58. Li S, Han Q, Qiao C, Song J, Cheng CL, Xu H. Chemical markers for the quality control of herbal medicines: an overview. Chin Med. 2008;3(1):1–16.
59. Colombo M, de Lima MG, Michels LR, Figueiró F, Bassani VL, Teixeira HF, Koester LS. Solid dispersion of kaempferol: formulation development, characterization, and oral bioavailability assessment. AAPS Pharm SciTech. 2019;20(3):1–9.
60. Hwang DH, Kim Y-I, Cho KH, Poudel BK, Choi JY, Kim D-W, Shin Y-J, Bae O-N, Yousaf AM, Yong CS. A novel solid dispersion system for natural product-loaded medicine: silymarin-loaded solid dispersion with enhanced oral bioavailability and hepatoprotective activity. J Microencapsul. 2014;31(7):619–26.

61. Kaur P, Singh SK, Garg V, Gulati M, Vaidya Y. Optimization of spray drying process for formulation of solid dispersion containing polypeptide-k powder through quality by design approach. Powder Technol. 2015;284:1–11.
62. Saokham P, Muankaew C, Jansook P, Loftsson T. Solubility of cyclodextrins and drug/cyclodextrin complexes. Molecules. 2018;23(5):1161.
63. Alopaeus JF, Hagesæther E, Tho I. Micellisation mechanism and behaviour of Soluplus®–furosemide micelles: preformulation studies of an oral nanocarrier-based system. Pharmaceuticals. 2019;12(1):15.
64. Solubility Enhancement with BASF Pharma Polymers. Solubilizer Compendium, Pharma Ingredients & Services: Lampertheim, Germany. 2011; https://pharmaceutical.basf.com/global/images/b_03_110921e_solubility_enhance_compendium.pdf.
65. Nair AR, Lakshman YD, Anand VSK, Sree KN, Bhat K, Dengale SJJAP. Overview of extensively employed polymeric carriers in solid dispersion technology. 2020;21(8):1–20.
66. Bide Y, Fashapoyeh MA, Shokrollahzadeh S. Structural investigation and application of Tween 80-choline chloride self-assemblies as osmotic agent for water desalination. Sci Rep. 2021;11(1):1–11.
67. Chen B, Wang X, Zhang Y, Huang K, Liu H, Xu D, Li S, Liu Q, Huang J, Yao H. Improved solubility, dissolution rate, and oral bioavailability of main biflavonoids from Selaginella doederleinii extract by amorphous solid dispersion. Drug Deliv. 2020;27(1):309–22.
68. Khan AW, Kotta S, Ansari SH, Sharma RK, Ali J. Enhanced dissolution and bioavailability of grapefruit flavonoid Naringenin by solid dispersion utilizing fourth generation carrier. Drug Dev Ind Pharm. 2015;41(5):772–9.
69. Zi P, Zhang C, Ju C, Su Z, Bao Y, Gao J, Sun J, Lu J, Zhang C. Solubility and bioavailability enhancement study of lopinavir solid dispersion matrixed with a polymeric surfactant-Soluplus. Eur J Pharm Sci. 2019;134:233–45.
70. Nitave SA, Chougule NB, Koumaravelou K. Formulation and evaluation of solid dispersion tablet of Andrographis paniculata extract. Pharmacog J. 2018;10(5).
71. Rehman S, Nabi B, Fazil M, Khan S, Bari NK, Singh R, Ahmad S, Kumar V, Baboota S, Ali J. Role of P-glycoprotein inhibitors in the bioavailability enhancement of solid dispersion of Darunavir. Biomed Res Int. 2017.
72. Liu P, Zhou J-Y, Chang J-H, Liu X-G, Xue H-F, Wang R-X, Li Z-S, Li C-S, Wang J, Liu C-Z. Soluplus-mediated diosgenin amorphous solid dispersion with high solubility and high stability: development, characterization and oral bioavailability. Drug Des Devel Ther. 2020;14:2959.
73. Slamova M, Školáková T, Školáková A, Patera J, Zámostný P. Preparation of solid dispersions with respect to the dissolution rate of active substance. J Drug Deliv Sci Technol. 2020;56: 101518.
74. Rashid R, Kim DW, ud Din F, Mustapha O, Yousaf AM, Park JH, Kim JO, Yong CS, Choi H-G,. Effect of hydroxypropylcellulose and Tween 80 on physicochemical properties and bioavailability of ezetimibe-loaded solid dispersion. Carbohydr Polym. 2015;130:26–31.
75. Beg S, Hasnain MS, Rahman M, Swain S. Introduction to quality by design (QbD): fundamentals, principles, and applications. In: Pharmaceutical quality by design. Elsevier. 2019;1–17.
76. Paidi SK, Jena SK, Ahuja BK, Devasari N, Suresh S. Preparation, in-vitro and in-vivo evaluation of spray-dried ternary solid dispersion of biopharmaceutics classification system class II model drug. J Pharm Pharmacol. 2015;67(5):616–29.
77. Dhillon N, Midha K, Nagpal M, Pahwa R. Formulation, optimization and characterization of solid dispersion of Glibenclamide. Pharm Methods. 2015;6(2).
78. Aulton ME, Taylor K. Aulton's pharmaceutics: the design and manufacture of medicines. 5th edn. Elsevier Health Sciences. 2018.
79. Ezawa T, Inoue Y, Tunvichien S, Suzuki R, Kanamoto I. Changes in the physicochemical properties of piperine/β-cyclodextrin due to the formation of inclusion complexes. Int J Med Chem. 2016.
80. Ezawa T, Inoue Y, Murata I, Takao K, Sugita Y, Kanamoto I. Characterization of the dissolution behavior of piperine/cyclodextrins inclusion complexes. AAPS Pharm SciTech. 2018;19(2):923–33.
81. Imam SS, Alshehri S, Alzahrani TA, Hussain A, Altamimi MA. Formulation and evaluation of supramolecular food-grade piperine HP β CD and TPGS complex: dissolution, physicochemical characterization, molecular docking, in vitro antioxidant activity, and antimicrobial assessment. Molecules. 2020;25(20):4716.
82. Stasiłowicz A, Rosiak N, Tykarska E, Kozak M, Jenczyk J, Szulc P, Kobus-Cisowska J, Lewandowska K, Płazińska A, Płaziński W. Combinations of piperine with hydroxypropyl-β-cyclodextrin as a multifunctional system. Int J Mol Sci. 2021;22(8):4195.
83. Zaini E, Fitriani L, Ismed F, Horikawa A, Uekusa HJSP. Improved solubility and dissolution rates in novel multicomponent crystals of piperine with succinic acid. 2020;88(2):21.
84. Lavra ZMM, Pereira de Santana D, Ré MI. Solubility and dissolution performances of spray-dried solid dispersion of Efavirenz in Soluplus. Drug Dev Ind Pharm. 2017;43(1):42–54.
85. Thakral NK, Ray AR, Bar-Shalom D, Eriksson AH, Majumdar DK. Soluplus-solubilized citrated camptothecin—a potential drug delivery strategy in colon cancer. AAPS Pharm SciTech. 2012;13(1):59–66.
86. Weerapol Y, Tubtimsri S, Jansakul C, Sriamornsak P. Improved dissolution of Kaempferia parviflora extract for oral administration by preparing solid dispersion via solvent evaporation. Asian J Pharm Sci. 2017;12(2):124–33.
87. Ding Y, Ding Y, Wang Y, Wang C, Gao M, Xu Y, Ma X, Wu J, Li L. Soluplus®/TPGS mixed micelles for co-delivery of docetaxel and piperine for combination cancer therapy. Pharm Dev Technol. 2020;25(1):107–15.
88. Lee J-Y, Kang W-S, Piao J, Yoon I-S, Kim D-D, Cho H-J. Soluplus®/TPGS-based solid dispersions prepared by hot-melt extrusion equipped with twin-screw systems for enhancing oral bioavailability of valsartan. Drug Des Devel Ther. 2015;9:2745.
89. Nanaki S, Eleftheriou RM, Barmpalexis P, Kostoglou M, Karavas E, Bikiaris D. Evaluation of dissolution enhancement of aprepitant drug in ternary pharmaceutical solid dispersions with Soluplus® and Poloxamer 188 prepared by melt mixing. Sci. 2019;1(2):48.
90. Zhang J, Lu A, Thakkar R, Zhang Y, Maniruzzaman M. Development and evaluation of amorphous oral thin films using solvent-free processes: comparison between 3D printing and hot-melt extrusion technologies. Pharmaceutics. 2021;13(10):1613.
91. Biswas S, Mukherjee PK, Kar A, Bannerjee S, Charoensub R, Duangyod T. Optimized piperine–phospholipid complex with enhanced bioavailability and hepatoprotective activity. Pharm Dev Technol. 2021;26(1):69–80.
92. Badria FA, Abdelaziz AE, Hassan AH, Elgazar AA, Mazyed EA. Development of provesicular nanodelivery system of curcumin as a safe and effective antiviral agent: Statistical optimization, in vitro characterization, and antiviral effectiveness. Molecules. 2020;25(23):5668.
93. Balata G, Shamrool H. Spherical agglomeration versus solid dispersion as different trials to optimize dissolution and bioactivity of silymarin. J Drug Deliv Sci Technol. 2014;24(5):478–85.
94. Nguyen MN-U, Van Vo T, Tran PH-L, Tran TT-D. Zein-based solid dispersion for potential application in targeted delivery. J Pharm Investig. 2017;47(4):357–64.

95. Lu Y, Tang N, Lian R, Qi J, Wu W. Understanding the relationship between wettability and dissolution of solid dispersion. Int J Pharm. 2014;465(1–2):25–31.
96. Salević A, Prieto C, Cabedo L, Nedović V, Lagaron JM. Physicochemical, antioxidant and antimicrobial properties of electrospun poly (ε-caprolactone) films containing a solid dispersion of sage (Salvia officinalis L.) extract. Nanomaterials. 2019;9(2):270.
97. Shah N, Iyer RM, Mair H-J, Choi D, Tian H, Diodone R, Fahnrich K, Pabst-Ravot A, Tang K, Scheubel E. Improved human bioavailability of vemurafenib, a practically insoluble drug, using an amorphous polymer-stabilized solid dispersion prepared by a solvent-controlled coprecipitation process. J Pharm Sci. 2013;102(3):967–81.
98. Agrawal AM, Dudhedia MS, Zimny E. Hot melt extrusion: development of an amorphous solid dispersion for an insoluble drug from mini-scale to clinical scale. AAPS Pharm SciTech. 2016;17:133–47.
99. Farmoudeh A, Rezaeiroshan A, Abbaspour M, Nokhodchi A, Ebrahimnejad P. Solid dispersion pellets: an efficient pharmaceutical approach to enrich the solubility and dissolution rate of deferasirox. Biomed Res Int. 2020.
100. Nandi U, Ajiboye AL, Patel P, Douroumis D, Trivedi V. Preparation of solid dispersions of simvastatin and soluplus using a single-step organic solvent-free supercritical fluid process for the drug solubility and dissolution rate enhancement. Pharmaceuticals. 2021;14(9):846.
101. Zhang Q, Polyakov NE, Chistyachenko YS, Khvostov MV, Frolova TS, Tolstikova TG, Dushkin AV, Su W. Preparation of curcumin self-micelle solid dispersion with enhanced bioavailability and cytotoxic activity by mechanochemistry. Drug Deliv. 2018;25(1):198–209.
102. Mohamed JMM, Alqahtani A, Ahmad F, Krishnaraju V, Kalpana K. Stoichiometrically governed curcumin solid dispersion and its cytotoxic evaluation on colorectal adenocarcinoma cells. Drug Des Devel Ther. 2020;4639–4658.
103. Song I-S, Cha J-S, Choi M-K. Characterization, in vivo and in vitro evaluation of solid dispersion of curcumin containing d-α-Tocopheryl polyethylene glycol 1000 succinate and mannitol. Molecules. 2016;21(10):1386.
104. Kuzu OF, Nguyen FD, Noory MA, Sharma A. Current state of animal (mouse) modeling in melanoma research. Cancer Growth Metastasis. 2015;8:CGM. S21214.
105. Kwon H-K, Hwang J-S, So J-S, Lee C-G, Sahoo A, Ryu J-H, Jeon WK, Ko BS, Im C-R, Lee SH. Cinnamon extract induces tumor cell death through inhibition of NFκB and AP1. BMC Cancer. 2010;10:1–10.
106. Kwon H-K, Jeon WK, Hwang J-S, Lee C-G, So J-S, Park J-A, Ko BS, Im S-H. Cinnamon extract suppresses tumor progression by modulating angiogenesis and the effector function of CD8+ T cells. Cancer Lett. 2009;278(2):174–82.
107. Zhang Q-Q, Zhou D-L, Ding Y, Liu H-Y, Lei Y, Fang H-Y, Gu Q-L, He X-D, Qi C-L, Yang YJMR. Andrographolide inhibits melanoma tumor growth by inactivating the TLR4/NF-κB signaling pathway. 2018;24(6):545–555.
108. Jin J-l, Gong J, Yin T-j, Lu Y-j, Xia J-j, Xie Y-y, Di Y, He L, Guo J-l, Sun J. PTD4-apoptin protein and dacarbazine show a synergistic antitumor effect on B16–F1 melanoma in vitro and in vivo. Eur J Pharmacol. 2011;654(1):17–25.
109. Surcel M, Constantin C, Caruntu C, Zurac S, Neagu M. Inflammatory cytokine pattern is sex-dependent in mouse cutaneous melanoma experimental model. J Immunol Res. 2017.
110. Li C, Han X. Co-delivery of dacarbazine and all-trans retinoic acid (ATRA) using lipid nanoformulations for synergistic antitumor efficacy against malignant melanoma. Nanoscale Res Lett. 2020;15(1):1–10.
111. Alexander A, Qureshi A, Kumari L, Vaishnav P, Sharma M, Saraf S, Saraf S. Role of herbal bioactives as a potential bioavailability enhancer for active pharmaceutical ingredients. Fitoterapia. 2014;97:1–14.
112. Nabekura T, Yamaki T, Ueno K, Kitagawa SJCC. Pharmacology Inhibition of P-glycoprotein and multidrug resistance protein 1 by dietary phytochemicals. Cancer Chemother Pharmacol. 2008;62:867–73.
113. Dudhatra GB, Mody SK, Awale MM, Patel HB, Modi CM, Kumar A, Kamani DR, Chauhan BN. A comprehensive review on pharmacotherapeutics of herbal bioenhancers. Sci World J. 2012
114. Malvi P, Chaube B, Singh SV, Mohammad N, Vijayakumar MV, Singh S, Chouhan S, Bhat MK. Elevated circulatory levels of leptin and resistin impair therapeutic efficacy of dacarbazine in melanoma under obese state. Cancer Metab. 2018;6(1):1–14.
115. Reid JM, Kuffel MJ, Miller JK, Rios R, Ames MM. Metabolic activation of dacarbazine by human cytochromes P450: the role of CYP1A1, CYP1A2, and CYP2E1. Clin Cancer Res. 1999;5(8):2192–7.